RICE UNIVERSITY

Nature and Evolution of Deep Water Carbonate Drifts in the past 3 Million years, Inner Sea of the Maldives Archipelago, Equatorial Indian Ocean.

by

Karem Lopez

A THESIS SUBMITTED
IN PARTIAL FULFILLMENT OF THE
REQUIREMENTS FOR THE DEGREE

Master of Science

APPROVED, THESIS COMMITTEE

Dr. André W. Droxler, Chair
Professor, Department of Earth Science

Richard G. Bodas, Chair for JBA

Dr. John B. Anderson
W. Maurice Ewing Professor in Oceanography, Department of Earth Science

Dr. Dale S. Sawyer
Professor, Department of Earth Science

HOUSTON, TEXAS
August 2012

RICE UNIVERSITY

Nature and Evolution of Deep Water Carbonate Drifts in the past 3 Million years, Inner Sea of the Maldives Archipelago, Equatorial Indian Ocean.

by

Karem Lopez

A THESIS SUBMITTED
IN PARTIAL FULFILLMENT OF THE
REQUIREMENTS FOR THE DEGREE

Master of Science

APPROVED, THESIS COMMITTEE

Dr. André W. Droxler, Chair
Professor, Department of Earth Science

Dr. John B. Anderson
W. Maurice Ewing Professor in Oceanography, Department of Earth Science

Dr. Dale S. Sawyer
Professor, Department of Earth Science

HOUSTON, TEXAS
December 2012

ABSTRACT

Nature and Evolution of Deep Water Carbonate Drifts in the past 3 Million years, Inner Sea of the Maldives Archipelago, Equatorial Indian Ocean.

by

Karem Lopez

The Maldives atolls, the very top of one of the largest modern carbonate platforms, occupy the central and largest part of the Chagos-Laccadives ridge located in the equatorial Indian Ocean. In the central part of the archipelago, the large atolls form two parallel north-south relatively continuous chains surrounding an internal basin, the Inner Sea, with water depths not exceeding 550 m. The Maldives carbonate system, uniquely evolved through a combination of global sea level fluctuations, subsiding history, and more regional seasonally varying monsoon circulation. Although the long-term evolution of this system is relatively well-established, the understanding of the detailed evolution of the Maldives carbonate edifice in the last 5 million years has remained limited. The latest phase of its stratigraphic evolution is explained by a shift from a well-developed Miocene-Pliocene progradational pattern to a mostly late Pliocene-Quaternary aggradational depositional signature. This last aggradation phase, forming the atolls the way we know them today, consists of stacked inner neritic limestone sequences, separated by a series of exposure horizons.

The successive periods of atoll exposure and re-flooding are recorded in the Inner Sea by late Pliocene-Quaternary glacial/interglacial clearly cyclic deposition of periplatform oozes. This cyclic sedimentary pattern also appears in the internal prograding geometry of carbonate drifts in the Inner Sea. A 200 m-thick deep carbonate sediment drift was first observed on a Shell E-W seismic line north of Gaafaru Falhu atoll in the NE corner of the Maldives Inner Sea, in a range of water depths from ~300 to 500 m. During the NEOMA 2007 research cruise on the RV *Meteor* lead by Universität Hamburg, the deep water sandy drift in the area north of Gaafaru Falhu atoll and an adjacent deeper muddy drift was extensively surveyed via 12 kHz multibeam bathymetry, a 4 kHz sub bottom profiler (Atlas Hydrographics), multi-channel high resolution seismics, and three box and piston cores.

My study focuses on understanding the Plio-Quaternary overall evolution of the set of adjacent sandy and muddy drifts, just north of Gaafaru Falhu Atoll. The sandy and muddy drift interconnected internal geometries observed in the available seismic data sets are integrated into a sequence stratigraphic framework. Analyses of two piston cores collected from the upper part of the muddy drift and a box core from the top of the sandy

drift determine the overall downcore lithology variations and made possible the development of high-resolution chrono and cyclo-stratigraphies. In the muddy drift periplatform sequence, downcore cyclic variations in, (1) sediment coarse fraction, (2) Sr counts as proxy for atoll-derived fine aragonite, (3) planktic foraminifer oxygen stable isotope composition, in addition to carbonate preservation and biostratigraphic markers, were determined. These downcore lithologic and geochemical variations in the muddy drift were tied to the seismic lines imaging the sandy-muddy drifts to resolve the timing of the carbonate sandy drift establishment and its overall evolution.

Based on this aforementioned interpretation, the results of my research document the nature and timing of the longer-term evolution of the sandy and muddy drifts over multiple glacial-interglacial sea level cycles in the last 3 million years. Once the timing of the drift was determined, the prograding internal architecture of the sandy drift was examined and interpreted in the context of the relatively well-established Plio-Pleistocene sea level fluctuations and the bottom current variations.

Acknowledgments

Completing this project would not have been possible without the assistance of so many people and institutions. The years I spent at Rice were truly an enjoyable experience. I would like to thank first my research advisor, Dr. André W. Droxler, who was a constant and enthusiastic source of encouragement, support, and advice throughout the past years. Dr. Droxler introduced me to the world of carbonate systems by proposing this challenging and fascinating thesis project. He also gave me the opportunity to attend several scientific meetings, which considerably enhanced my understanding of carbonate stratigraphy. His help during the writing up phase of this thesis is particularly appreciated. I have benefited immensely from his professional wisdom. Moreover I would like to thank my thesis committee members, Dr. John B. Anderson and Dr. Dale S. Sawyer for their guidance during the different stages of my graduate research.

I am grateful to all my fellow peers, Lizette Leon R., Rodrigo Fernandez, Becky Minzoni, Jeniffer Masy, Alex Kirshner, Brandon Harper, and Ayca Agar, for their continued support, with a special thanks to Maria A. Bravo for her amazing collaboration on the preparation of the samples. I would like to thank the wonderful administrative and technical staff at the Earth Science department especially the support of Soookie S., Sandra F., Mary Ann L., Lee W., Roger R., Pat J., Bonnie H., and many other staff members when it came to meeting the bureaucratic requirements of graduate school and submitting a thesis.

I am very grateful to Professor Mark Leckie, at University of Massachusetts, College of Natural Sciences, who made important contributions to this project. He

provided intense training on foraminifer identification, skills that were essential to develop high resolution oxygen isotope stratigraphy that became the backbone of my thesis. I would also like to thank Dr. Howard Spero, at the University of California, the Department of Geology, to analyze numerous samples for oxygen and carbon isotopes.

I owe a special thank to colleagues and friends at Lumina Geophysical, LLC, for their contribution in reprocessing seismic lines, which made possible a convincing correlation between the core stratigraphy and lithological downcore variations and the seismic images of the deep water juxtaposed muddy and sandy drifts. The US-National Foundation (Marine Geology and Geophysics-IODP; Award Number: 0729070) and Total (Oil and Gas Company), for funding my project. A special thanks to Dr. Philippe Lapointe at Total.

I would like to acknowledge the collaboration with Prof. Christian Betzler and Dr. Jörn Fürstenau from the University of Hamburg, my communication with them ranged from scientific exchange to generously sharing important data sets. Lastly, I would like to thank Dr. Ursula Rohl, Thomas Westerhold, and Lukies Vera from MARUM, at University of Bremen. I have benefited immensely from their professional wisdom. They gave me access to laboratory equipment, software, and computer that enhanced my productivity while I XRF scanned two of my cores.

This project would not have been possible without the support of my family. I thank my husband Carlos for his understanding and support during my graduate studies and our beautiful twin daughters, Annabelle and Annette, for their unconditional love and patience.

Contents

List of Figures

List of Tables

1. Introduction

The Maldives atolls, the very top of one of the largest modern carbonate platforms, form the central and largest part of the Chagos-Laccadives ridge located in the equatorial Indian Ocean (Fig.1). Since the Maldives platform has been far from any terrigenous influence for its 50 my-long history, this 2-3 km-thick edifice is composed almost entirely of carbonate sediments. These modern atolls are part of the latest evolution phase of this platform, which initially established itself on top of an early Eocene subsiding volcanic plateau (Aubert and Droxler, 1996; Aubert and Droxler, 1992; Belopolsky and Droxler, 2003; Purdy and Bertram, 1993). In carbonate system evolution, sediment production and accumulation, local tectonic, eustatic sea level, and climate variability primarily control their observed stratigraphic sequences and neritic carbonates and facies patterns. The facies structure of carbonate shelves and platforms, therefore, reflects the combined effect of at least three of these parameters (Kendall and Schlager, 1981; Schlager, 2005). The Maldives carbonate system, because of its location in the equatorial Indian Ocean, uniquely evolved through a combination of global sea level fluctuations, subsiding history, and more regional seasonally varying monsoon circulation. Because the Maldives carbonate platform is located in a tectonic stable mid-ocean setting within the Indian plate, it has the potential for providing an excellent record of sea level fluctuations, particularly during late Pliocene-Quaternary high frequency and high amplitude oscillations, in spite of the strong influence of the monsoonal circulation and its seasonal current reversal (Aubert and Droxler, 1996; Aubert and Droxler, 1992; Belopolsky and Droxler, 2003; Betzler et al., 2012; Betzler et al., 2009; Droxler et al., 1990; Purdy and Bertram, 1993; Sarkar and Gupta, 2009; Woodroffe, 2005; Woodroffe,

2008). Recently, Betzler et al. (2009 and 2012) have shown that the combination of sea level fluctuations and the monsoonal bottom current variability has generated a series of periplatform sandy and muddy carbonate drifts in the Maldives Inner Sea since the middle Miocene.

My research focuses on understanding the Plio-Quaternary overall evolution of a set of juxtaposed sandy and muddy drifts in the northeast corner of the Maldives Inner Sea, just north of Gaafaru Falhu Atoll (Figs. 2A & B). New multi-beam and seismic data sets, two piston cores and one box core were collected in my study area during the 2007 NEOMA expedition on the R/V *Meteor*. The sandy and muddy drift interconnected internal geometries from the available seismic lines allow to understand the overall evolution of this set of drifts, placing it into a sequence stratigraphic framework. Analyses of two piston cores, collected from the upper part of the muddy drift, and a box core, from the top of the sandy drift, give excellent opportunities to determine the overall downcore lithology variations and the development of high-resolution chrono and cyclo-stratigraphies for the upper part of the drifts. Similar stratigraphies developed at ODP Site 716 (Droxler et al., 1990), located 7 km approximated northwest of the study area, help to develop the full evolution of the drifts and place it in a chronologic framework. The linkage between cores and seismic data is essential to understand how sedimentologic and oceanographic processes influenced the evolution of the drifts in particular in relationship with late Plio-Quaternary sea level fluctuations and bottom current variations. Based on this aforementioned interpretation, I am able to document the nature and timing of the longer-term evolution of the sandy and

muddy drifts over multiple glacial-interglacial sea level cycles in the last three million years or so.

2. The Maldives Geographical, Climatic and Oceanic Settings

The Maldives Archipelago consists of a group of atolls located in the equatorial Indian Ocean, southwest of India, and occupies the central part of the Chagos-Laccadives Ridge. The elongated string of atolls, 900-km long and 130 km wide, stretches for about 8 degrees in latitudes on a north-south orientation from $7^0$06'N (Ihavandippolu Atoll) to $0^0$42'S (Addu Atoll) (Fig.1). Although the total surface area of the Republic of Maldives covers 107,500 km^2, only 298 km^2 consist of exposed land with an average elevation of 1.5 meters above sea level. The current exposed land, therefore, represents a tiny fraction of the submerged 2-3 km thick and geographically extensive Maldives carbonate mega-platform that has existed since the early Eocene (Belopolsky and Droxler, 2004b; Nicora and Silva, 1990).

The Maldives Archipelago consists of approximately 2000 distinct small coral reefs grouped into 25 major atolls (Naseer and Hatcher, 2004), circular or elongated in shape and a couple to tens of kilometers in diameter. In the central part of the archipelago ($5^0$30'N and $2^0$30'N), the large atolls form two parallel north-south relatively continuous chains surrounding an internal basin, the Inner Sea, with water depths not exceeding 550 m in the North to 400 m in the South and is locally 40-60 km wide (Fig. 1B) (Aubert and Droxler, 1996).

Air temperatures in the Maldives range between 24^0C and 33^0C throughout the year. Mean annual temperature approximates 28^0C, with little seasonal variation. Water temperatures are relatively constant, ranging from 25 to 29^0C (Purdy and Bertram, 1993). The Maldives Archipelago is affected by a monsoon-triggered seasonal reversing current regime (Tomczak and Godfrey, 2003). The summer monsoon, corresponding to the rainy season, occurs from June to October and is characterized by some of the strongest winds blowing predominantly northeastward. In contrast, the winds during the winter monsoon (dry season) blow predominantly southwestward from December to April (Betzler et al., 2009; Purdy and Bertram, 1993).

The seasonal monsoonal wind circulation also generates oceanic currents. Surface currents in January are westerly in the northern part of the archipelago and easterly in its southern part; during July, they become generally easterly but are weak throughout. Tidal ranges that are mainly semi-diurnal vary from 0.7 m in the north to almost 1 m in the south (Purdy and Bertram, 1993).

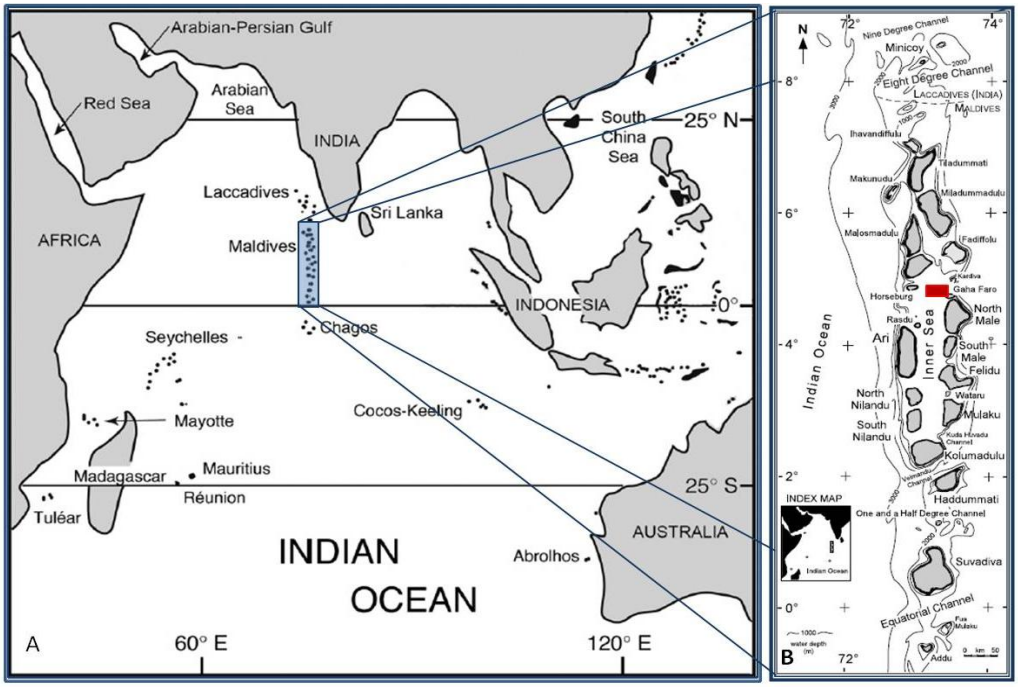

Figure 1. A. General location of The Maldives Archipelago in the Indian Ocean (modified from Gischler, et al., 2008). B. Detailed of the string of atolls in the Maldives Archipelago, Study area is located in the red rectangle (modified from Belopolsky and Droxler, 2004b).

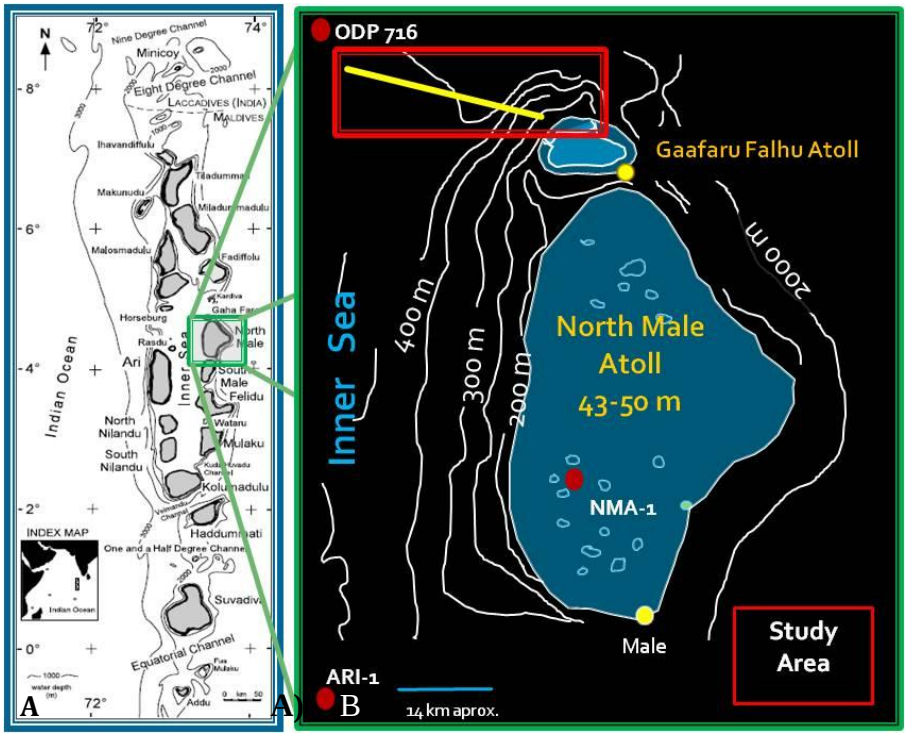

Figure 2. **A.** Maldives Archipelago (modified from Belopolsky and Droxler, 2004b). **B.** Details of North Male and Gaafaru Falhu Atoll bathymetry and study area location (modified from Aubert and Droxler, 1996).

3. The Maldives Geological Setting

3.1 Neogene Evolution of the Carbonate Edifice

The general geological evolution of the Maldives carbonate system is surprisingly well established because hydrocarbon exploration in the Maldives was already initiated in the early 1970's. Numerous 2D seismic surveys were acquired both in the Inner Sea and in the atoll lagoons by Elf Aquitaine. In 1976, Elf Aquitaine drilled a deep exploration well NMA-1 inside the North Malé atoll lagoon (Fig. 2B). The well penetrated a 2106 m-thick succession of Eocene to Pleistocene carbonates overlying a 116 m-thick sequence

of weathered 55 Ma old basalts, dated by Ar/Ar (Duncan and Hargraves, 1990). Based upon these data sets, Aubert and Droxler (1992-1996), Purdy and Bertram (1993) developed a first framework to explain the overall evolution of the Maldives carbonate system.

Ocean Drilling Program (ODP) drilled three sites in the Maldives in 1987; Sites 714 and 715, drilled on the toe of slope of the Maldives carbonate edifice, target its early evolution. At Site 715, the volcanic basement was recovered and dated (Backman et al., 1988; Belopolsky and Droxler, 2003; Duncan and Hargraves, 1990) and the initial establishment of the neritic carbonates in the early Eocene was determined based upon Larger benthic foraminifer biostraigraphy by Nicora and Silva (1990). Site 716, drilled in the northern part of the Inner Sea, recovered 262 m of Quaternary-to-late-Miocene periplatform oozes and chalks (Backman et al., 1988; Malone et al., 1990). In 1989, Royal Dutch Shell acquired a tight grid of high resolution seismic lines limited to the Inner Sea and in 1991 drilled ARI-1 well in the central part of the Inner Sea (southeast of Ari Atoll) at 348 m of water depth (Fig. 2B). The well encountered 3315 m of late Eocene to modern carbonates and recovered 50 m of weathered basalts (Aubert and Droxler, 1996; Belopolsky and Droxler, 2004b). Based on the interpretation of this additional seismic and well data sets, Belopolsky and Droxler (2003/2004a), improved the overall understanding of the 55-57 My long term evolution of the Maldives carbonate mega-platform, initially developed by Aubert and Droxler et al. (1992 and 1996) and Purdy and Bertram, 1993).

3.2 Quaternary Evolution of the Carbonate Edifice

The understanding of the Quaternary detailed evolution of the Maldives carbonate edifice has remained limited. Aubert and Droxler (1996) interpreted the latest phase of the Maldives carbonate system stratigraphic evolution by a shift from Miocene-Pliocene systematic progradational pattern to a Quaternary mostly aggradational depositional signature (Fig. 3A). This last aggradation phase in the atolls consists of stacked inner neritic limestone sequences, separated by a series of exposure horizons (Gischler et al., 2008).

The modern atoll physiography in the Maldives can be explained by the interaction of high frequency and high amplitude sea level fluctuations in the last 3 My but in particular during the last 0.5 My (Fig. 3). Early Pliocene flat-topped carbonate banks became mostly exposed during the late Pliocene and early Pleistocene through a long interval of systematically falling sea-level, and remained exposed most of the time for about 2 My (Fig. 3B). In the early Pleistocene, the exposed banks might have been also briefly re-flooded at ~ 1.0 Ma, 1.5 Ma, and ~ 2.0 Ma (Fig. 3C). During these sucessive exposures, karst topographies were developed on the shallow bank tops. This complex karst morphology ultimately developed during the early Brunhes became the substratum for reef development during a series of five, 120 m plus high amplitude, mid to late Brunhes sea level rises and falls; the atolls physiography, such as the one we observe today, became prevalent. The latest development of the Maldivian carbonate system provides a clear illustration of the antecedent-karts theory (Fig. 3B), (Purdy, 1974a; Purdy and Bertram, 1993).

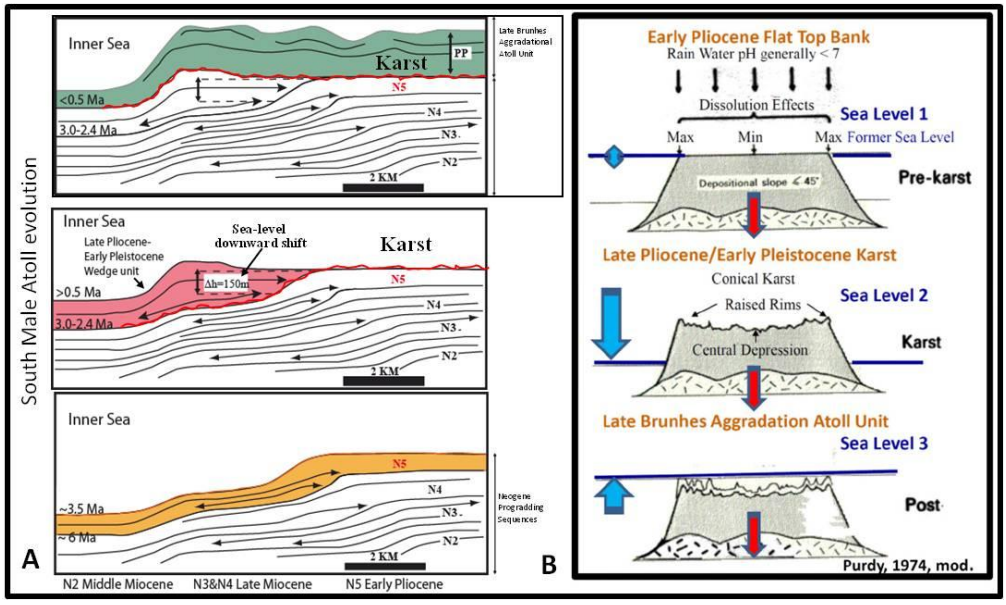

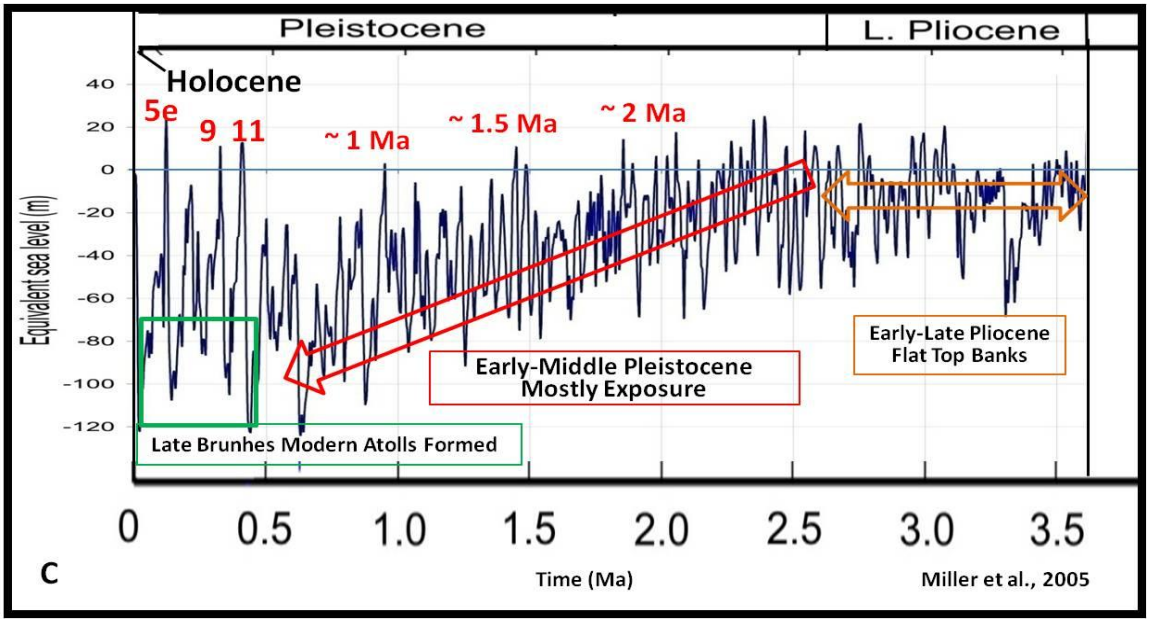

Figure 3. Models for the atoll formation in the Maldives Archipelago. **A.** Illustrated the latest phase of the Maldives stratigraphic evolution; from systematic progradational pattern (N1-N5) to a Quaternary aggradational depositional signature (green shaded interval). **B.** Early Pliocene flat-topped banks mostly exposed during late Pliocene to early Pleistocene and therefore, karstified during a long term systematic sea level fall during the early and middle Pleistocene (**C**) Sea level curve in (**C**) from Miller et al.,

2005. The modern atoll formed during the periodic reflooding of karstic morphology since the mid-Brunhes (**C**) MIS 11,9, 5e and 1. Early phases of atoll formation may have ocurred during highstand sea levels intervals at about 1, 1.5 and 2 million years (**C**). This model could be a good illustration of the "Antecedent Karst Theory" developed by Purdy (1974) (**B**).

Succesive periods of atoll exposure and re-flooding is recorded in the Inner Sea by the Quaternary and in particular middle-late Brunhes glacial/interglacial clearly cyclic deposition of periplatform oozes in particular at Site 716 (Droxler et al., 1990; Malone et al., 1990; Reymer et al., 1988). This cyclic sedimentary pattern also appears in the internal prograding geometry of carbonate drifts in the Inner Sea. For instance, a 200 m-thick deep carbonate sediment drift was first observed on a Shell E-W seismic line north of Gaafaru Falhu atoll in the NE corner of the Maldives Inner Sea, in a range of water depths from ~350 to 500 m (Belopolsky and Droxler, 2004). These authors realized that this 200m-thick deep water drift most likely accumulated rapidly in the Quaternary. During the NEOMA 2007 research cruise on the RV *Meteor* lead by Universität Hamburg, the area north of Gaafaru Falhu atoll was extensively surveyed via 12 kHz multi-beam bathymetry, a 4 kHz sub bottom profiler (Atlas Hydrographics), and multi-channel high resolution seismic (Figs. 4&5). Based on these surveys, the drift has been clearly imaged in three dimensions.

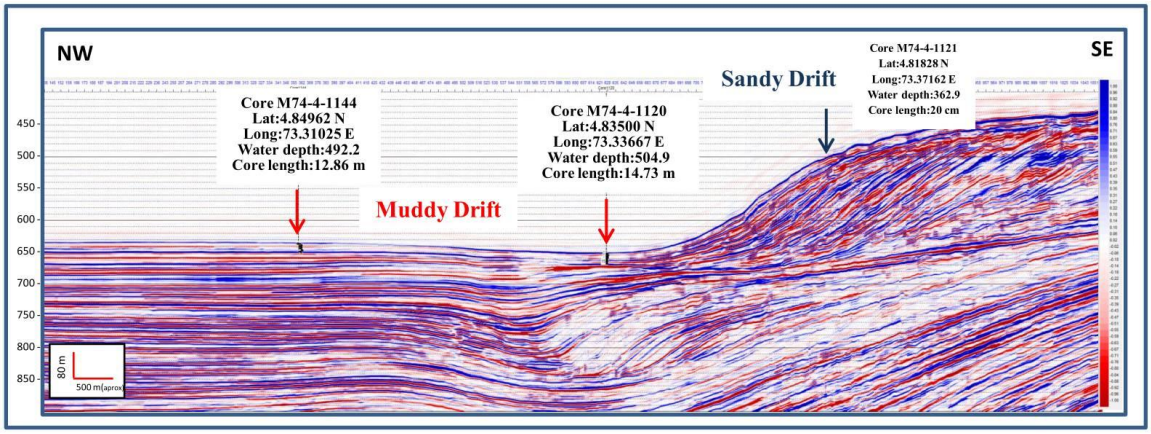

Figure 4. Ultra spectral inversion high resolution seismic at 300 Hz re-procesed by Lumina, Geophysical (Puryear and Castagna, 2008). Uninterpreted P4 segment, showing cores data and location. Seismic data adquired during NEOMA Research Cruise 2007.

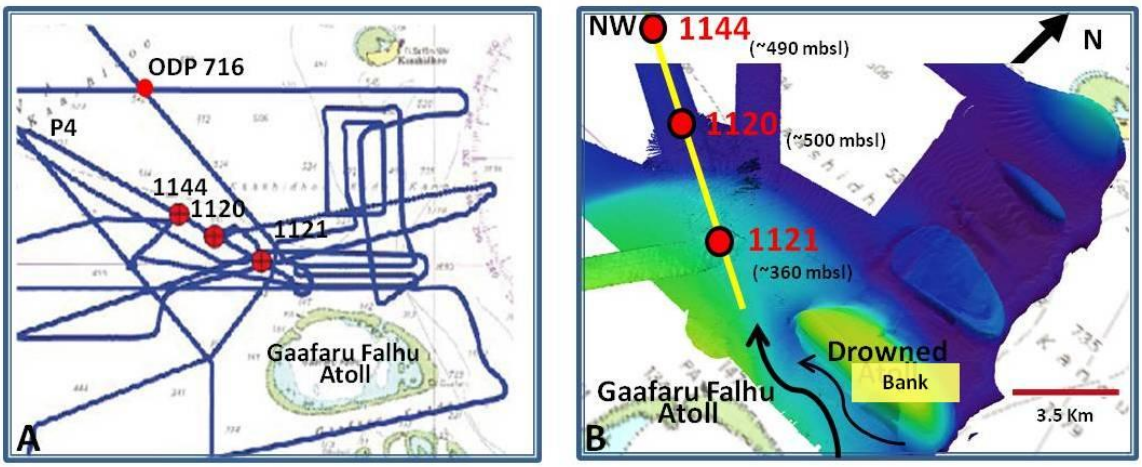

Figure 5. **A**. Core locations: piston cores M74-4-1120 and M74-4-1144, M74-4-1121 box core, and ODP Site 716. Blue lines: available multi-channel seismic and sub-bottom profiler lines. **B**. Multi-beam bathymetric map of the study area (NEOMA cruise, 2007, unpublished data).

The drift has accumulated at the western exit of a deep channel located north of Gaafaru Falhu atoll (Fig. 5B, Betzler et al., 2009). The 4 km-wide and 350 m deep

channel is bounded on its north side by the southern margin of a drowned platform and on its southern side by the northern margin of Gaafaru Falhu atoll (Fig. 5B; refer also to figure 1 in Betzler et al., 2012). Strength of the westerly current flowing through the channel, illustrated by very high sand waves observed within the channel axis, is tied to the winter Indian monsoon circulation (Betzler et al., 2009).

3.3 Tectonic Setting

The equatorial Indian Ocean is known for unique intraplate deformation (DeMets et al., 2005; Gordon et al., 1998). A broad region of deforming oceanic lithosphere in the central Indian Ocean acts as a diffuse oceanic plate boundary between two distinct tectonic plates, the Indian and Capricorn Plates (Fig. 6). The motion between those two plates since 8 Ma appears steady with little indication of episodic motion. Since the present motion across the central Indian basin began no earlier than 11 Myr (Gordon et al., 1998), the Maldives carbonate platform has been positioned on the rigid part of the Indian Plate for at least the past 11 Myr and is located several hundreds of kilometers away from the diffuse plate boundaries. Therefore, the Maldives carbonate platform was not directly affected by intraplate deformation; it explains the relative absence of noticeable seismic activity in the area since the late Oligocene.

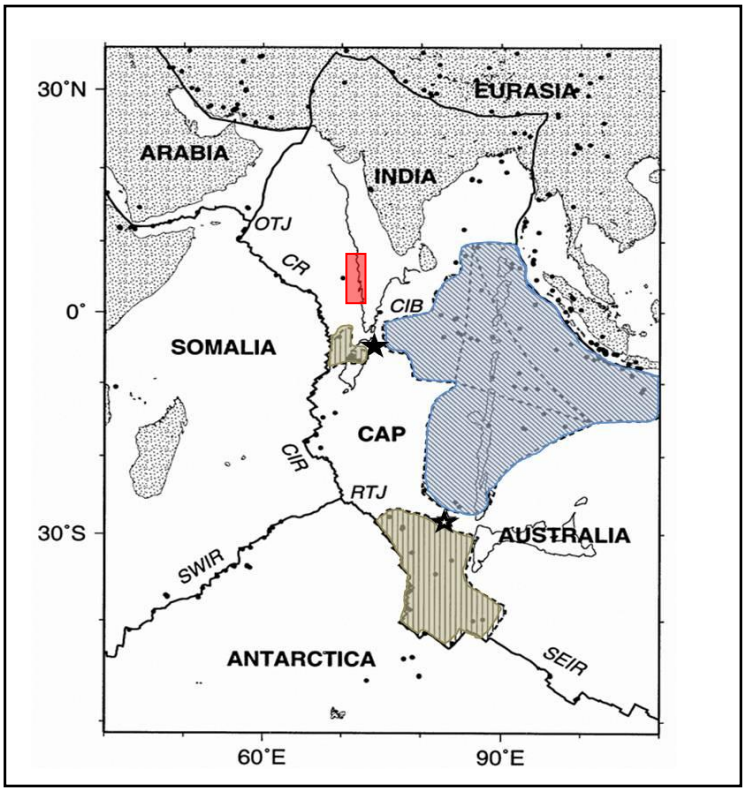

Figure 6. Map shows in the central Indian Ocean a broad region of deforming oceanic lithosphere which acts as a diffuse oceanic plate boundary between Indian and Capricorn plates. Vertically striped regions (green shadow) are diffuse plate boundaries across which divergence is accommodated; the diagonally striped region (blue shadow) shows diffuse plate boundaries across convergence is accommodated. CAP, Capricorn plate; OTJ Owen triple junction; CR, Carlsberg ridge; CIB, central Indian basin; CIR, central Indian ridge; RTJ, Rodrigues triple junction; SEIR, southeast Indian ridge; SWIR, southwest Indian ridge. Modified from Gordon et al., 1998. Red box shows an aproximate location of the Maldives Archipelago.

4. Data Sets

Piston and box cores, multi-channel seismic lines, sub-bottom profiles, and multi-beam bathymetry were acquired during the NEOMA research cruise on the R/V *Meteor* leg M74/4, in December 2007 (Figs. 5A&B). This research program is a collaboration with Prof. Christian Betzler at Hamburg University and Prof. John Reijmer at the Free University of Amsterdam.

4.1 Cores Data

During the NEOMA cruise, two piston cores M74-4-1120 and M74-4-1144, in addition to one box core M74-4-1121, were retrieved on top of the muddy and sandy drifts north of Gaafaru Falhu Atoll, in the northeastern part of the Maldives Inner Sea (Fig. 5). Piston cores 1120 and 1144, in water depths of 505 and 492 m recovered the upper part (14.73 and 12.86 m, respectively) of the muddy drift; the box core 1121 recovered the top 20 cm of the sandy drift at a water depth of 353 m (Table 1). As shipboard analyses, the cores were visually described and scanned for downcore color and lightness variations based upon which a preliminary stratigraphy was developed.

Coring Devices	Core Name	Core Legth (m)	Position		
			Longitude (dec.deg)	Latitude (dec. deg)	Water Depth (mbsl)
Box Core	M74-4-1121	0.2	73.37162 E	4.81828 N	352.9
Piston Core	M74-4-1144	12.86	73.31025 E	4.84962 N	492.2
Piston Core	M74-4-1120	14.73	73.33667 E	4.83500 N	504.9

Table 1. Information about cores used in this study.

4.2 Multi-Channel Seismic Data

Based on the NEOMA cruise report (www.dfg-ozean.de), multi-channel 2D high-resolution seismic lines were generated by means of two clustered GI-Guns, each with a volume of 45 in^3 for a 105 in^3 generated injector. A digital 144-channel streamer array

with an active length of 600 m and an asymmetric group interval was used. Data sets were digitized by seven SeaMUX 24 channel 24-bit digitizing modules, configured in six multiple arrays totaling 144 channels. The selected shooting distance during the entire cruise was 12.5 m. The dominant frequencies center around 100-120 Hz. The vertical resolution equals approximately 4-6 m. Depths on seismics are approximated using an average sonic velocity of 1600 m/s (Ludmann, T., personal communication).

4.3 Sub-bottom-profiler Data

A hull-mounted Parasound system (Atlas Hydrographics) generated very high-resolution seismic images down to maximum 100 m sub-seafloor. From the two frequencies emitted (18 and 22 kHz), a 4-kHz signal is generated in the water column due to the parametric effect. The vertical resolution is to estimated to be one meter or less.

4.4 Multi-beam Bathymetry Data

Multi-beam imaging was performed with a hull-mounded EM710 multi-beam echosounder (Kongsberg Maritime). The EM710 is a high-resolution mapping system with 256 simultaneous beams operating in the 70-100 kHz range and covering a swath width of up to 5.5 times water depth. Depth resolution is at centimeter to decimeter scale. The beams are stabilized for roll, pitch, and yaw. Data obtained were post-processed using the software package Neptune. Visualization of surfaces and extraction of atoll margin morphology were conducted using the software package Fledermaus (IVS 3D), at a lateral grid resolution of 5 m (Furstenau et al., 2009).

5. Sample Processing and Analyses

5.1 Sample Preparation

The piston cores were systematically sub-sampled by pushing in 24 ml tubes along the core half sections at 5-10 cm intervals. 411 samples were analyzed for size fractions, micropaleontology, and stable oxygen-isotopes. Box core sediments were analyzed for size fraction.

Each sample volume could be determined because it was collected using identical syringe tubes and, therefore, density of the samples could be calculated. Bulk samples were first wet weighted, oven-dried at 75°deg. C for 24 hr, and then weighted as dried samples. Bulk dried samples were placed in a buffered solution of phosphate (pH 7.5) for 24 hr and washed over a 63μm screen to separate coarse sediment fraction (> 63 μm) from fine sediment fraction (< 63 μm). The two size fractions were dried in an oven at ~ 75° deg. C, weighted and transferred into labeled plastic vials. The > 63 μm size fraction masses were subtracted from those of bulk samples to determine the percentage coarse sediment in the sample and were split into equal aliquots, using a micro-splitter. Half of the coarse fraction was sieved through a set of two 300 and 250-μm screen sieves. The fraction between 250 and 300 μm size ranges was examined using a Leica MZ6 stereomicroscope to extract foraminifers for stable oxygen isotopes and identify foraminiferal biostratigraphy markers. The other half was preserved as archives for future analyses. Elements composition was determined through XRF analyses on the archive half sections at 1 and 0.5 cm intervals (see below).

5.2 Stable Isotope Analysis

Planktic stable oxygen isotopes were determined in 304 samples from both piston cores at samples intervals ranging from 5 to 10 cm. 20-25 specimens of planktic foraminifer *Globigerinoides ruber* (white) were hand-picked from the 250 to 300 μm size fraction using a binocular microscope (Leica MZ6).

Samples were placed in a small glass bottle, filling it half way with methanol, and ultrasonically cleaned for about 7 seconds to remove potential fine-fraction sediment contamination. Stable oxygen isotope analyses were performed at the University of California, Davis (UCD), using a GV Instruments Optima mass spectrometer. Isotope values are reported in delta notation relative to V-PDB reference and have an analytical precision of ±0.06‰.

5.3 Fluorescence Analysis

Archives half core sections covering the uppermost 14.00 and 12.57 m of cores 1120 and 1144, respectively, were run through the AVAATECH (XRF Core Scanner III) core scanner at MARUM, University of Bremen. The X-ray Fluorescence (XRF) core scanner is designed for rapid and non-destructive determination of chemical composition of marine bottom sediments.

XRF Core Scanner III data were collected every 1 cm down-core over a 1 cm^2 area with slit size of 1 cm using generator settings of 50 and 10 kV, a current of 1.0 and 0.20 mA respectively, and a sampling time of 30 seconds directly at the split core surface of the archive half. The split core surface was covered with a 4 micron-thin SPEXCerti

Prep Ultralene foil to avoid contamination of the XRF measurement unit and desiccation of the sediment. The core surface was slightly smoothed for soft sediment cores, whereas for hard sediments, a smooth roller was used to squeeze out air bubbles and water under the film. The data, reported further in this study, have been acquired by a Canberra X-PIPS Silicon Drift Detector (SDD; Model SXD 15 C-150-500) with 150eV X-ray resolution, the Canberra Digital Spectrum Analyzer DAS 1000 and an Oxford Instruments 100W Neptune X-ray tube with rhodium (Rh) target material. Raw data spectra were processed by the Analysis of X-ray spectra by Iterative Least square software (WIN AXIL) package from Canberra Eurisys. Element intensities were measured in total counts (cnts). Data acquired from a setting of 50 kV corresponds to Sr and Ba, whereas Ca, Si, Fe and K elements from a setting of 10 kV.

A 3CCD High Speed Color Line Scan Camera CV-L107 integrated in the XRF Core Scanner system was used for color scanning. The cores were scanned in meter sections at 1 cm down-core spacing measurements and were saved in different image formats. Sr counts are a valuable proxy for bank-derived fine aragonite content (Dunbar and Dickens, 2003) usually measured by X ray Diffraction (XRD). As an explanation, large cations, such as Sr are preferentially substituted for Ca in orthorhombic aragonite, whereas small cations such as Mg are preferentially substituted for Ca in rhombohedral calcite. Sr counts are can easily be determined using an X-ray Fluorescence (XRF) Core Scanner, at 1 cm, even 0.5 cm spaced intervals.

5.4 Pteropod Preservation Index

Carbonate (aragonite) preservation index was estimated based on the whole pteropods. It was considered fragmented pteropod if more than half of the shell was broken. Analyses were determined on sieved samples >300 ųm size fraction. Pteropods data are presented as Percent whole pteropods= $\frac{\#\ Whole\ pteropods}{\#whole+\#\ fragmented\ pteropods} * 100$. 300 whole or fragmented pteropod tests were counted for each sample (Haddad and Droxler, 1996).

5.5 Biostratigraphy

An integrated age model for the cores was established based on a high-resolution dating method using planktic foraminifer and biostratigraphic markers.

The chronology control on both cores is based on the relative abundance of the planktic pink-pigmented foraminifers *Globigerinoides ruber*, an important fossil marker of the Indian and Pacific Oceans (Thompson et al., 1979). Planktic foraminifers (*G. ruber* pink) were identified from both cores, using a binocular microscope Leica MZ6 from samples in 250-300 μm size fractions. Samples were examined to identify the pink first and last *G. ruber* occurrence down the cores (Zheng et al., 2005), occurring within MIS 14 and at the end of the transition from MIS 6 to 5 (or Termination II) (Thompson et al., 1979), respectively.

6. Results and Interpretation

6.1 Core Sediment Analyses

The 20 cm-thick sediment unit recovered in box core 1121 on the very top of the sandy drift corresponds to unlithified carbonate grainstones with 90% sand size grains. Two third of the 20 cm box core sediment, correspond to coarse sand (355-1000 μm), mostly skeletal angular atoll derived shell fragments and benthic foraminifers. The other third of the sand, between 63-355 μm, is a mixture of planktic foraminifers, pteropods, skeletal atoll derived fragments, and benthic foraminifers (Fig. 7).

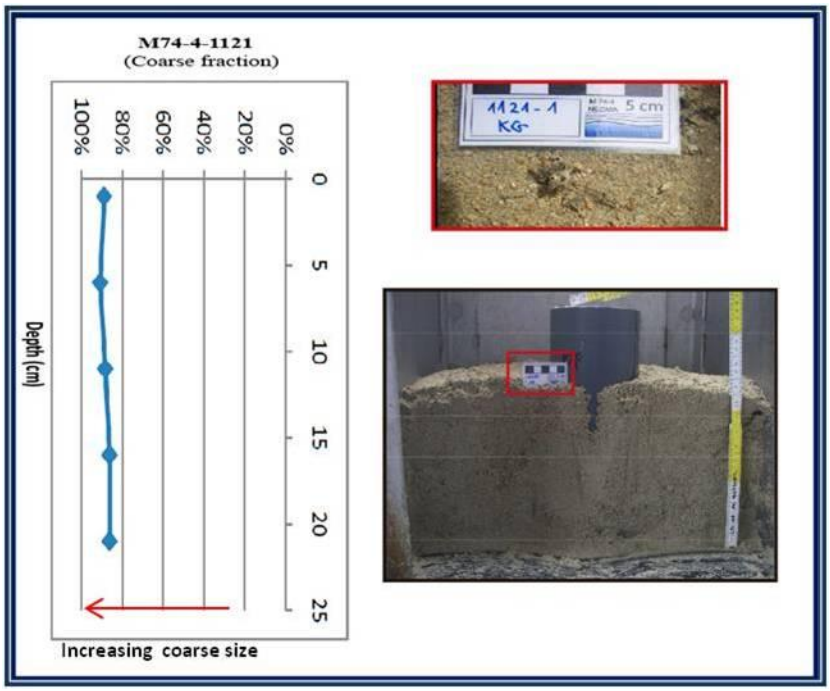

Figure 7. Box core M74-4-1121. The box core recovered 20 cm from the surface of the carbonate sand drift. The two third of the box core sediments, correspond to coarse sand (355-1000 μm), mostly skeletal angular shell fragments and benthic foraminifers.

Both piston cores (M74-4-1120 and M74-4-1144) display downcore alternating intervals of coarse and fine periplatform ooze (Figs. 8A & 9A). Thicker intervals, significantly expended by dilution of fine (< 63 μm) atoll derived Sr-rich, therefore aragonite sediments, alternate with thinner condensed intervals characterized by high coarse sediments fraction (> 63 μm) values, ranging between 25-90 % in both cores, and Sr-low sediment. The coarse sediments analyzed consist primarily of planktic foraminifers and pteropods and contains minimal benthic constituents, such as deep benthic foraminifers, sponge, echinoderm fragments, and ostracods. Atoll derived shallow benthic foraminifers and other neritic grains are rare occurrences.

Strontium contents values throughout core 1120 range from 3000 to 16400 counts displaying a regular cyclic pattern down the core. In core 1144, strontium counts, systematically higher than in core 1120, vary cyclically down core from 5200 to 20190 counts. These high resolution downcore variations of strontium (Sr) counts, an excellent proxy for atoll bank-derived fine aragonite (Dunbar and Dickens, 2003) (Figs. 8B & 9B), display in cores 1120 and 1144 a cyclic pattern generally in phase with coarse sediment fraction. The relationship between Sr counts and grain size demonstrates that high Sr counts values corresponds to low coarse sediment fraction and vice versa.

Figure 8C shows the downcore variations of the pteropods (aragonite) fragmentation index (Whole Pteropods / Whole Pteropods + Fragments). An interval of unusually high pteropods fragments (usually 50% or lower) occurs downcore from about 7 to 12 m, contrasting with the low pteropods fragmentation (above 50%) between 12 and 14 m, and 1.4 and 7 m. This possible longer cycle does not appear to be linked to the

observed higher frequency cycles in the downcore coarse fraction and Sr count variations.

Both cores 1120 and 1144 display a clear downcore high frequency cyclic pattern in planktic foraminifer oxygen isotope from -1 and – 2.5 per mil (Figs. 8D & 9C). These cycles appear to be in phase with the downcore variations of strontium counts and coarse sediments fraction (Figs. 8 & 9).

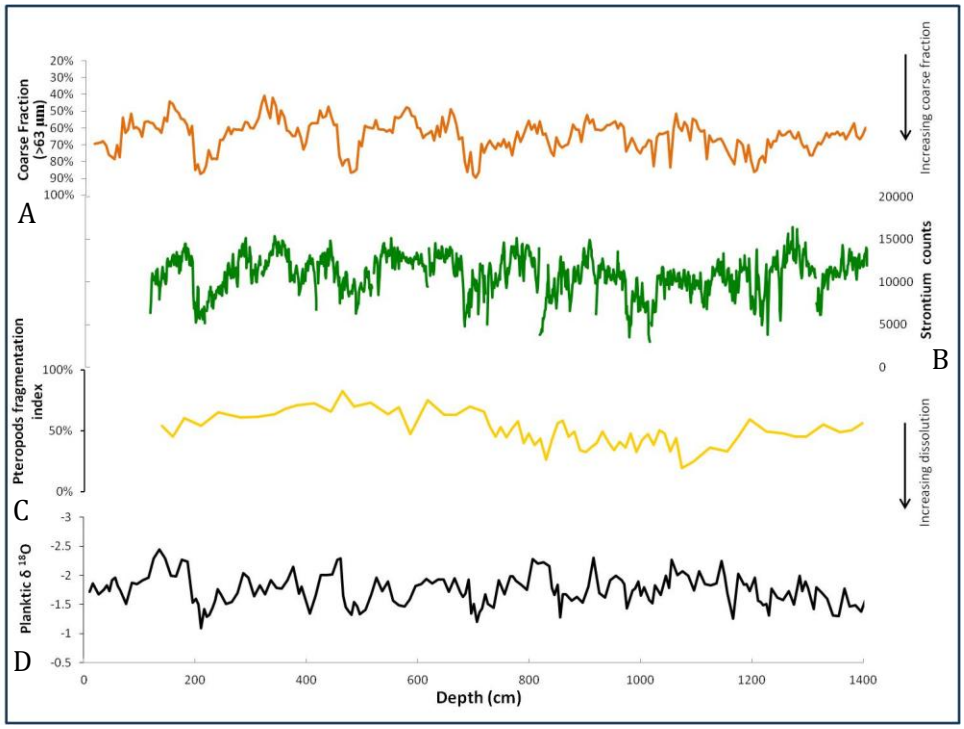

Figure 8. Results of Piston core M74-4-1120, sediment analysis relative to core depth (14.73 m). **A.** Coarse sediments fraction (%); note inverted scale. **B.** Strontium counts. **C.** Pteropods fragmentation index; note high pteropod fragments yield low % index values. **D.** Planktic foraminifer (*G. ruber* white 250 – 300 µm) stable oxygen isotope curve.

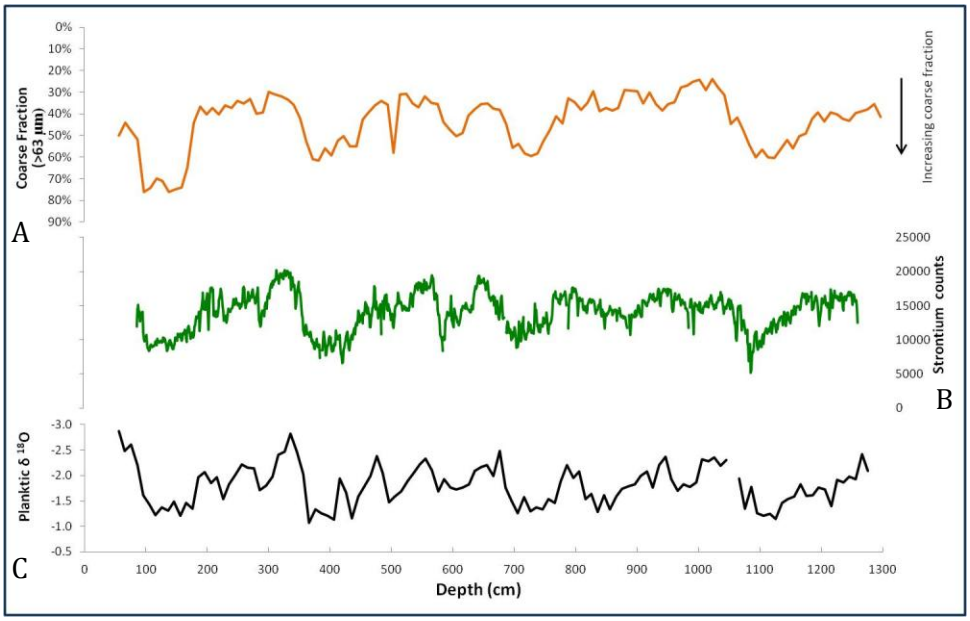

Figure 9. Results of Piston core M74-4-1144, sediment analysis relative to core depth (12.86 m). **A.** Coarse sediments fraction (%); note inverted scale. **B.** Strontium counts. **C.** Planktic foraminifer (*G. ruber* white 250 – 300 µm) stable oxygen isotope curve.

6.1.1 Age/Depth Model

Stable oxygen isotope data (*G. ruber,* (white)), produced in both piston cores 1120 and 1144 (Figs. 8D & 9C), are correlated in figures 10 with the well-dated stacked benthic foraminiferal oxygen isotope (LR-04) curve of Lisiecki and Raymo (2005). 18 MIS $\delta^{18}O$ events, defined and tied to a specific age on LR 04 stacked curve were identified on cores 1120 and 1144 (see Tables 2 and 3; Fig. 10).

Based upon these events, depths to age models were developed for both cores, assuming a constant sedimentation rates for the core interval between two MIS events. Then, the depth to age models are tested when the planktic $\delta^{18}O$ records are plotted on time and on top of the LR04 stacked $\delta^{18}O$ curve (Fig. 11). The match between the

planktic records and the LR04 stacked benthic curve is remarkable for both cores 1120 and 1144 (Figs. 11A & B).

Upon this visual comparison and excellent match, the bottom of core 1120 is interpreted to represent the initiation of glacial MIS 18, and, therefore, the core has recovered a sediment interval representing about the last 750 ky (Figs.10A & 11A) or almost the entire Brunhes period. As shown in figure 11A, this interpretation is anchored by available biostratigraphic markers, in agreement for instance with the disappearance of the *G. ruber* (pink) at the transition from MIS 6 to MIS 5e (or Termination II) (Thompson et al., 1979), and the first appearance of the *G. ruber* (pink) within the MIS 14 (Zheng et al., 2005).

A depth-to-age model, based on LR-04, MIS events, similar as the one applied to core 1120, was developed for core 1144 (Figure 10B). The bottom of core 1144 at 12.86 m is interpreted to occur at the beginning of the second part of MIS 11, representing event MIS 11.24 or 391 ky. The strength of the depth-to-age model for core 1144 is verified in plotting on time core 1144 planktic $\delta^{18}O$ record on top of the LR04 stacked benthic $\delta^{18}O$ curve (Fig. 11B). The match between the two records is as remarkable as the match for core 1120. The depth-to-age model for core 1144 is consistent with the level in the core were *G. ruber* (pink) disappear at the transition from MIS 6 to 5e (Termination II) (Fig. 11B).

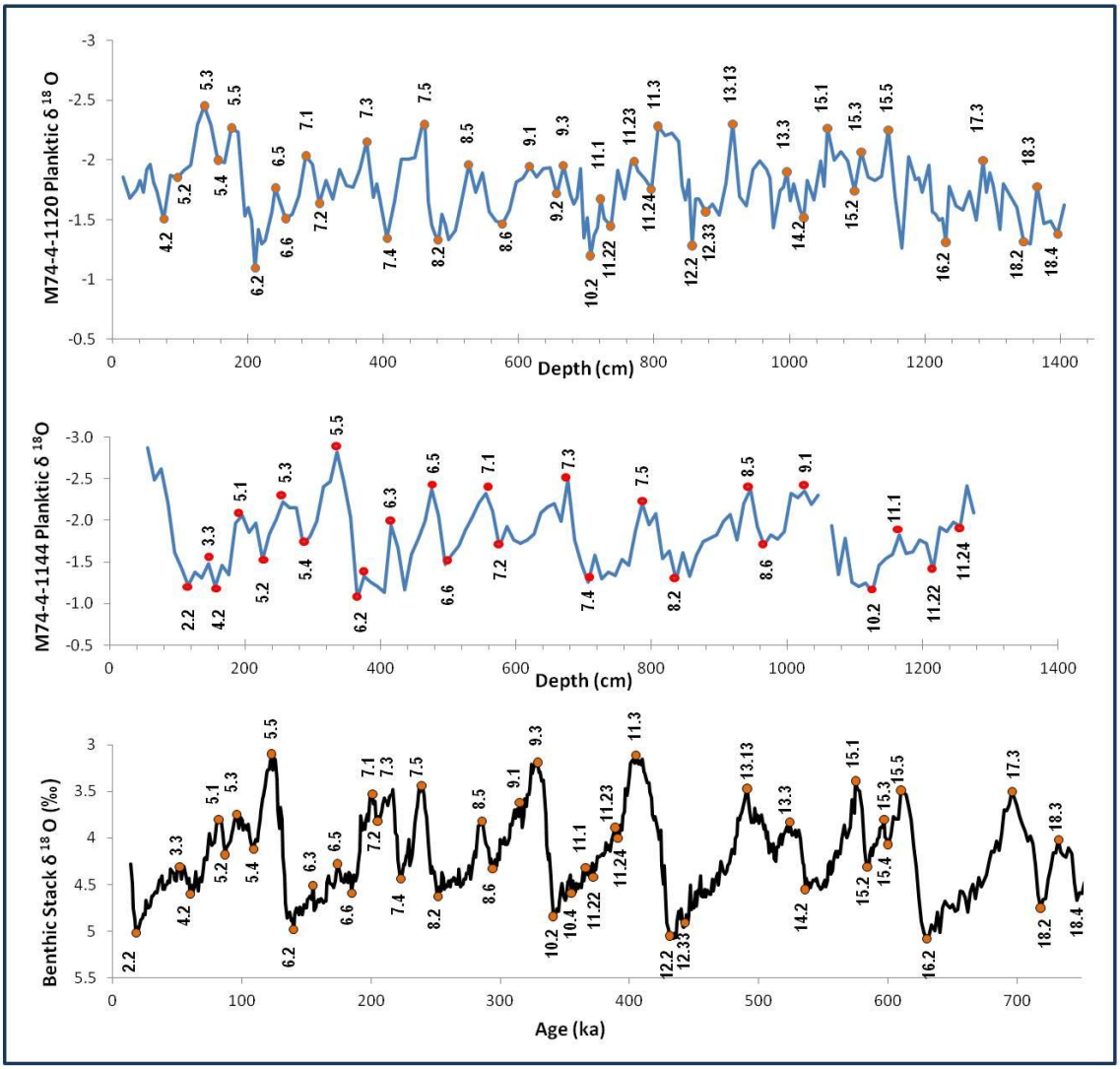

Figure 10. Piston cores M74-4-1120 and M74-4-1144 depth/age correlation with the well-dated stacked benthic foraminiferal oxygen isotope curve of Lisiecki and Raymo (2005).

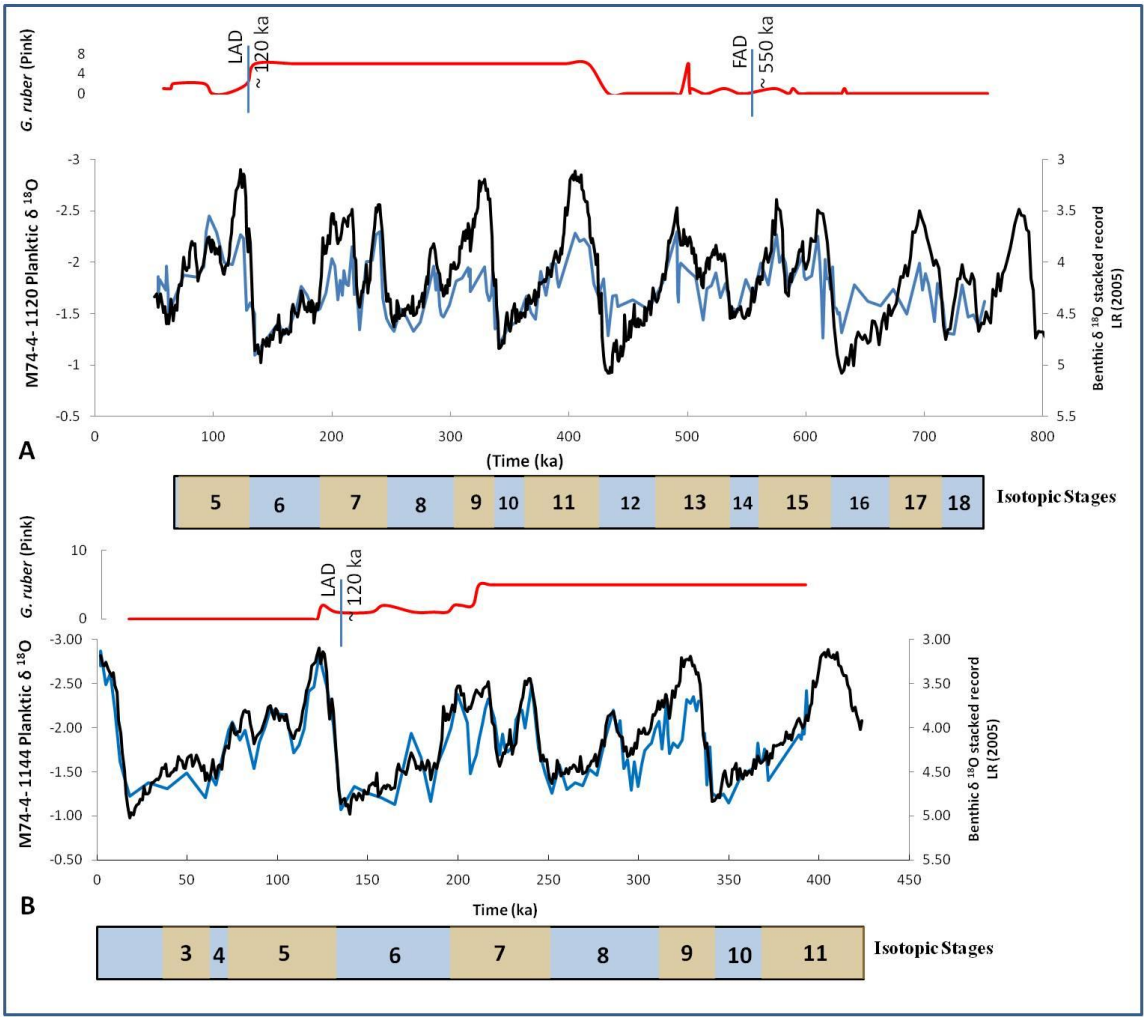

Figure 11. Stable isotope data from cores M74-4-1120 (**A**) and M74-4-1144 (**B**) (blue lines) correlated with the well-dated stacked benthic foraminiferal oxygen isotope (black lines). Red lines corresponds to biostratigraphic marker *G. ruber* (pink).

Because the lengths of cores 1144 and 1120 are quite similar, 12.8 and 14 m, respectively, although the age of the oldest sediments in core 1120 at 745 ky is almost twice as old as the age of oldest sediments in core 1144 at 391 ky, the sedimentation rates in core 1144 are, therefore, roughly twice as high as the ones in core 1120.

M74-4-1120		
MIS Events	**Depth (cm)**	**Age (ka)**
4.2	76	62
5.2	96	87
5.3	136	96
5.4	156	109
5.5	176	123
6.2	211	135
6.3	216	155
6.5	241	174
6.6	256	185
7.1	286	200
7.2	306	205
7.3	376	217
7.4	406	223
7.5	456	237
8.2	481	252
8.5	526	286
8.6	576	294
9.1	616	315
9.2	656	317
9.3	666	329
10.2	706	341
11.1	721	364
11.22	736	372
11.23	771	389
11.24	796	391
11.3	806	405
12.2	856	433
12.33	876	441
13.13	916	491
13.3	996	524
14.2	1016	536
15.1	1056	575
15.2	1096	585
15.3	1106	597
15.4	1126	600
15.5	1146	610
16.2	1231	630
17.3	1286	696
18.2	1346	718
18.3	1366	732
18.4	1396	746

M74-4-1144		
MIS Events	**Depth (cm)**	**Age (ka)**
2.2	116	18
4.2	156	62
5.1	216	82
5.2	226	87
5.3	256	96
5.4	286	109
5.5	336	123
6.2	366	135
6.5	416	174
6.6	436	185
7.1	476	200
7.2	486	205
7.3	556	217
7.4	576	223
7.5	666	237
8.2	706	252
8.5	786	286
8.6	826	294
9.1	936	315
9.2	966	317
9.3	1016	329
10.2	1096	341
11.1	1146	364
11.22	1216	372
11.23	1226	389
11.24	1246	391

Table 2. MIS events from the benthic stacked record of LR 2005 identified in cores M74-4-1120 (left) and M74-4-1144 (right), and their corresponding core depths and respective ages based upon which the age/depth models were developed in both cores (Figures 10 and 11). Blue areas correspond to interglacial MIS intervals.

In Figure 12, occurrence of MIS events in core depth are plotted versus time for piston cores 1120 and 1144. In this figure, the slopes of the curves correspond, therefore, to the variations through time of the sedimentation rates and clearly demonstrate that the highest sedimentation rates systematically occur during interglacial intervals (in blue), whereas lowest sedimentation rates characterized glacial intervals (in white). In piston cores 1120 and 1144, lowest sedimentation rates range from ~0.25 to 1.4 cm/ky and ~0.5 to 2.3 cm/ky, respectively, in glacial intervals. The highest sedimentation rates in both piston cores 1120 and 1144 range from a ~ 10 to 15 cm/ky and ~ 12.5 to 20 cm/ky, respectively, during interglacial intervals. Overall, the sedimentation rates are about twice higher in piston core 1144 than in 1120. This observation can be explained by the individual location of the cores relative to the muddy drift. Piston core 1120 is located within the muddy drift moat where westward bottom currents are expected to be the highest. In this context, fine sediments, mostly winnowed within the moat, are preferentially transported and ultimately deposited towards the central part of the muddy drift where piston core 1144 is located.

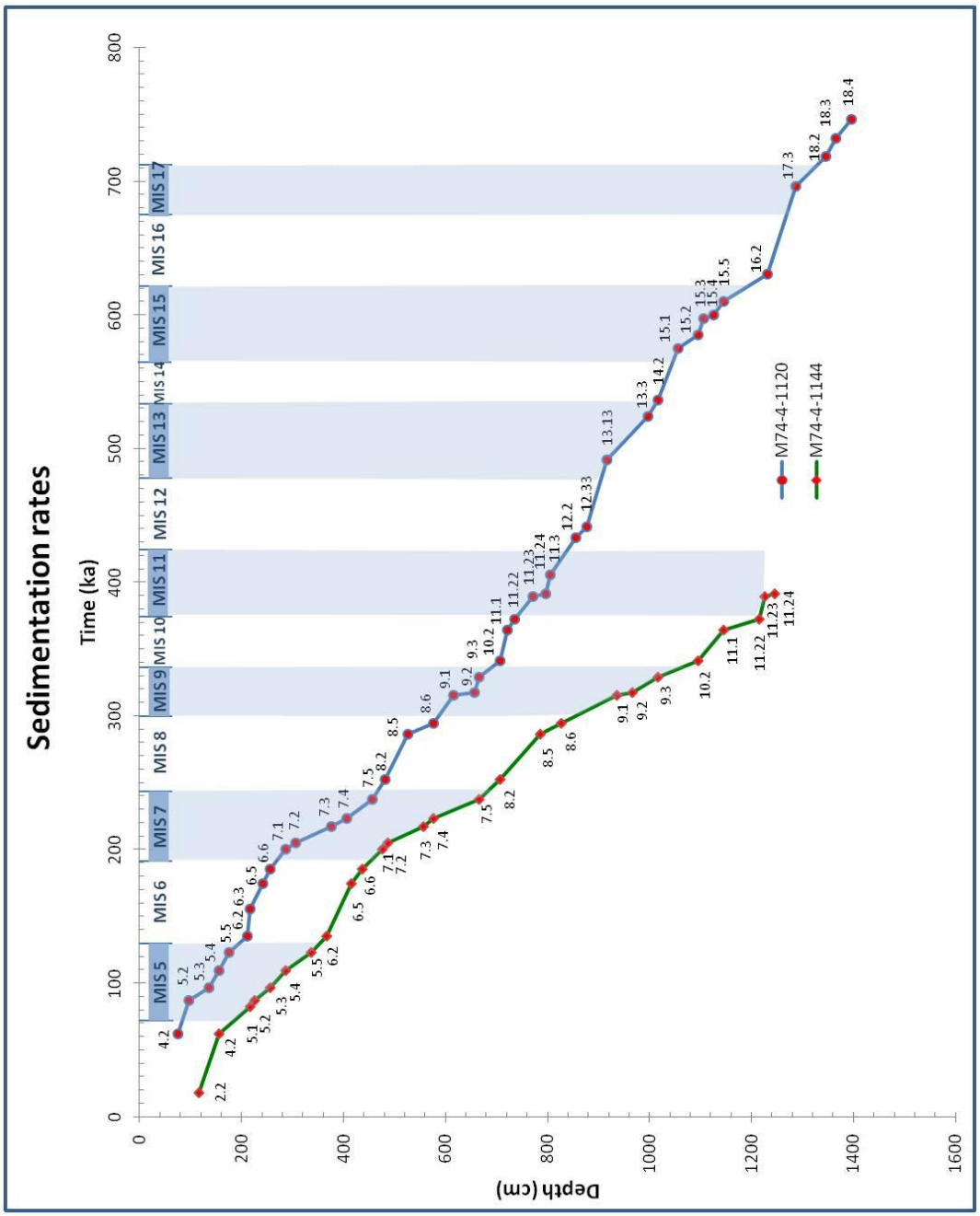

Figure 12. Age/depth curve of piston cores M74-4-1120 and M74-4-1144 illustrating the variable glacial and interglacial sedimentation rates. The highest sedimentation rates are systematically occurring during interglacial intervals, represented by blue shaded areas.

6.1.2 Interpretation of Sediment Analyses

Based on a depth/age model, resulting from the correlation between the planktic foraminiferal isotope records and the well-dated stacked benthic foraminiferal oxygen isotope (LR-04) curve of Lisiecki and Raymo (2005), results of the sediment analyses can be interpreted. The complete results from both cores 1120 and 1144 are shown relative to time in figures 13 and 14. Coarse sediment fraction variations in time display a clear glacial-interglacial cyclic pattern in both cores (Figs. 13B & 14B) when compared with the LR04 stacked benthic oxygen isotope curve. Low coarse sediment fraction values correspond to interglacial intervals, whereas glacial stages, are represented by condensed intervals of high coarse sediment fraction. The overall amplitudes of the coarse sediment fraction cycles in core 1120 increase during the Brunhes, from low to intermediate and high amplitudes during the early, mid, and late Brunhes. In core 1144, high amplitude sediment coarse fraction cycles are observed in the late Bruhnes as in core 1120. In core 1144, the coarse sediment fraction values gradually increase through the late Brunhes.

High resolution downcore variations of Sr counts versus time display, in cores 1120 and 1144, a cyclic glacial-interglacial pattern generally in phase with cores 112 and 1144 planktic foraminifer oxygen isotope records and, therefore, the LR04 stacked benthic foraminifer oxygen isotope curve. Sr content values throughout core 1120, (Fig. 13D) illustrate an average interglacial strontium values that range from 10000-12000 counts and the glacial values from 7000-8000 counts.

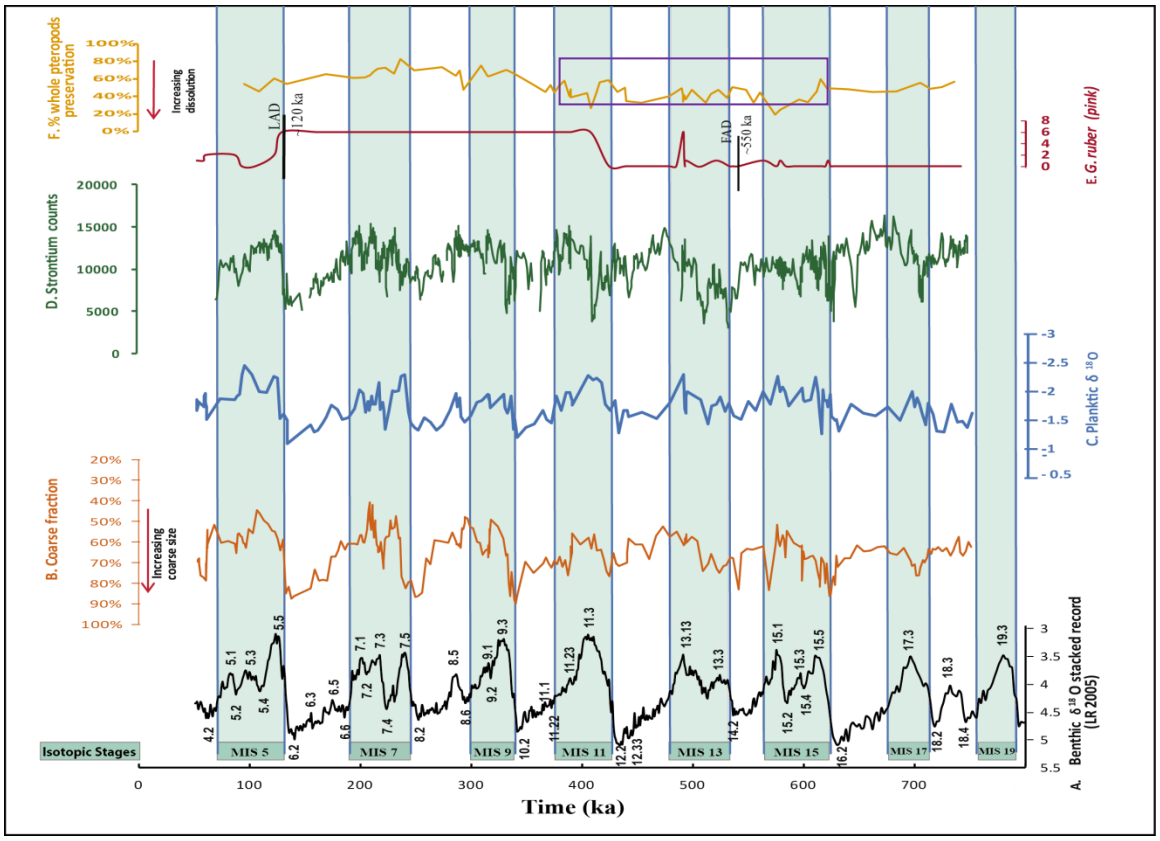

Figure 13. Piston core M74-4-1120 results. **A.** Benthic $\delta^{18}O$ stacked record shows Pleistocene climatic cycles, (Lisiecki and Raymo, 2005). **B.** Downcore coarse fraction % variations (> 63μm) Note inversed vertical axis. **C.** Planktic oxygen isotope record based upon analysis of *Globigerinoides ruber (white).* **D.** High resolution downcore variations of strontium counts. **E.** % relative abundance of the *G. ruber* (pink); disappearance of *G. ruber* (pink) marks the transition from MIS6 to MIS5e (Thompson et al., 1979); its first appearance identifies the beginning of MIS 14 (Zheng et al., 2005). **F.** Proxy of carbonate dissolution, based on pteropods preservation; purple box corresponds to the maximun dissolution interval. Glacial/interglacial cycles are clearly illustrated down to MIS 18. Interglacials are represented by blue shaded intervals.

In core 1144 (Fig. 14D), strontium counts, systematically higher than in core 1120, vary cyclically down core, with average interglacial values range from 17000-20000 counts and average glacial values from 7000-10000 counts.

The in phase strong relationship between Sr counts and planktic $\delta^{18}O$, high Sr count values corresponding to light interglacial $\delta^{18}O$ ratios and low Sr count values to heavy glacial $\delta^{18}O$ ratios, is especially clear during the late Brunhes (the last three glacial cycles) in both cores 1120 and 1144 (Fig. 15); however this relationship becomes tenuous in the early and middle Brunhes. In the late Brunhes, therefore, the highstand shedding concept (Schlager et al., 1994) is clear in cores 1120 and 1144.

Carbonate sediment accumulation is essentially driven by sea-level and is largely related to highstand shedding in tropical carbonates (Schlager et al., 1994). Sea-level fluctuations influence the carbonate mineralogy of the slope and basin periplatform sediment through alternately flooding and exposing the shallow banktops (Boardman et al., 1986; Droxler et al., 1983). Bank-derived aragonite, therefore Sr-rich, fine sediment increases in periplatform sediments, when carbonate platform flat tops are flooded and their production and export reach their maxima during sea-level highstands and ceases during lowstands when platform tops are exposed and karstified.

In cores 1120 and 1144, the maximum Sr-rich fine sediment accumulation on the Inner Sea drifts occurred, in reference with Miller et al. (2011) sea level curve, when atoll tops were flooded during the late Brunhes interglacial sea-level highstands. During these times, export of fine bank-derived Sr-rich neritic aragonite sediments towards the adjacent slopes and basins was maximum (Figs. 15 and Fig. 16A&D). This export reached minima during glacial sea-level lowstands when the atoll lagoon was exposed and therefore karstified (Fig. 15 and Fig. 16C&E).

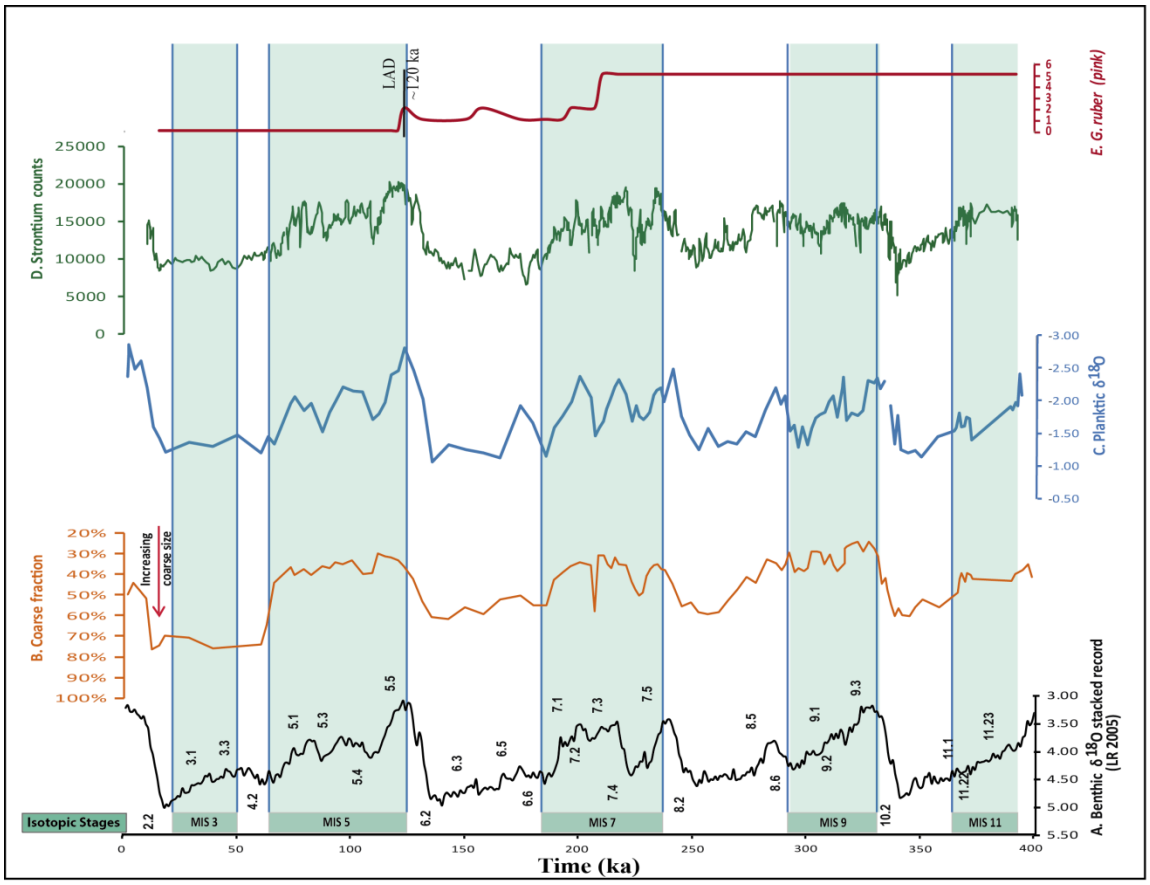

Figure 14. Piston core M74-4-1144 results. **A**. Benthic $\delta^{18}O$ stacked record shows late Pleistocene climatic cycles, (Lisiecki and Raymo, 2005). **B.** Downcore coarse fraction % variations (> 63 μm) display a clear cyclic patterns. Note inversed vertical axis. **C.** Marine Isotope Stages can be easily identified in the stable oxygen isotope record based upon analysis of *Globigerinoides ruber (white)* down to stage MIS 11. **D**. High resolution downcore variations of strontium counts. E. % relative abundance of the *G. ruber (pink);* disappearance of *G. ruber (pink)* marks the transition from MIS6 to MIS5[e] (Thompson et al., 1979). Glacial/interglacial are clearly illustrated down to MIS 11. Interglacials are represented by blue shaded intervals.

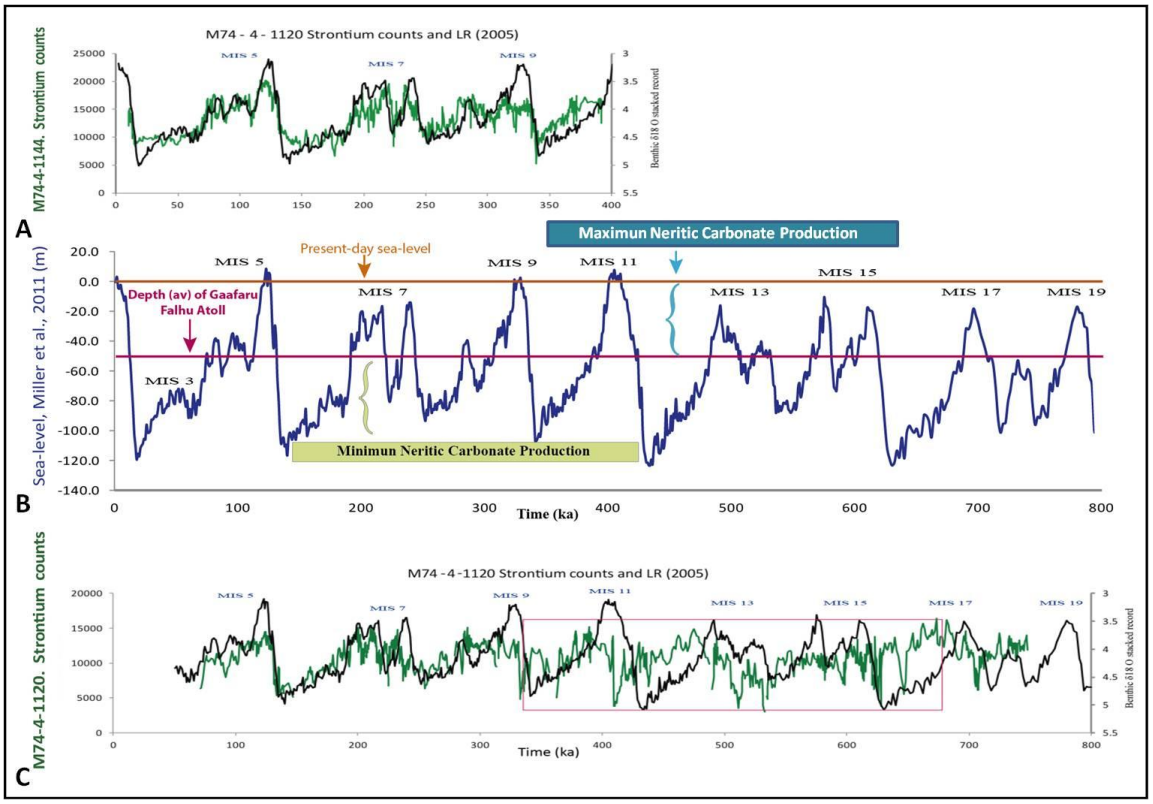

Figure 15. Comparison of Strontium counts from both cores (M74-4-1144 and M74-4-1120) with sea-level fluctuations (Miller et al., 2011).

The late Brunhes in phase relationship between Sr and $\delta^{18}O$ is not clearly observed earlier during the early and middle Brunhes in core 1120 (Fig. 15C). At some specific intervals, this relationship appears totally out of phase. The highest Sr counts in core 1120 occur in the first parts of glacial MIS 16 and 13, whereas the lowest Sr counts are centered during the first half of interglacial MIS 13 and 11 (Fig. 15C). The sea level highstand shedding concept, adequate to explain the last three late Brunhes glacial-interglacial sea level cycles, can obviously not be applied to justify some of the lowest Sr counts at times when sea level was established to be high, such as during the sea level highstand peaks of MIS 11 and 13 (Fig.15B&C).

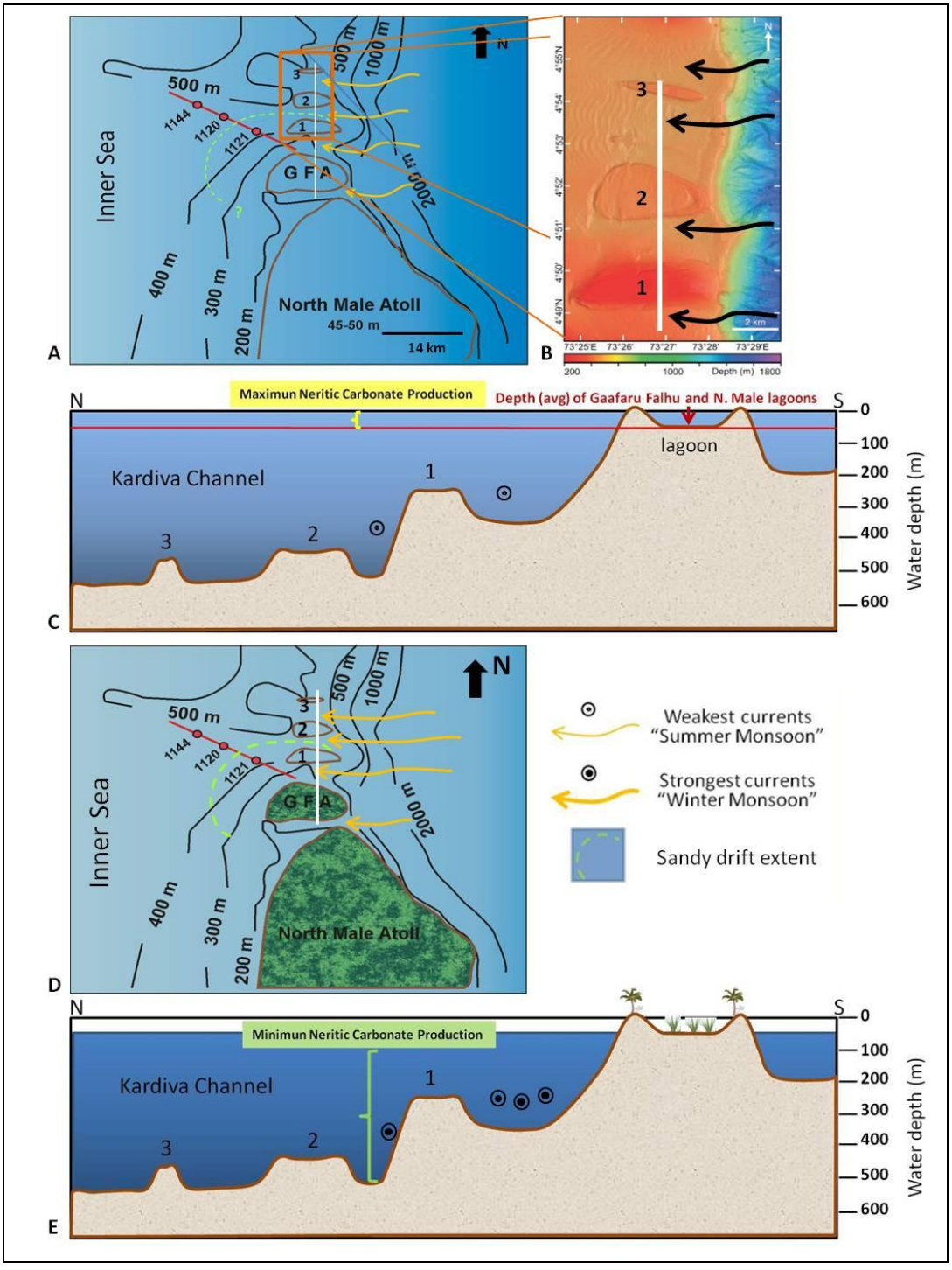

Figure 16. Schematic diagrams to illustrate interglacial (highstand) and glacial (lowstand) highstand shedding scenario. Interglacial high neritic carbonate production and export occur when the atoll lagoons are flooded, building the adjacent carbonate sandy and muddy drifts. During glacial intervals, the carbonate neritic production was drastically diminished because the atoll lagoons were exposed. Stronger currents generated by more

intense winter monsoon easterly winds partially eroded the upper parts of the sandy drift. **A-B-C.** Modern bathymetry and schematic cross section of the study area including North Male/Gaffaru Falhu Atolls in the south and the drowned banks (# 1-3; Betzler et al., 2009) in the north side, separated by a series of E-W channels. **D-E.** Schematic representations of the glacials/lowstand situation when N. Male and Gaffaru Falhu lagoon were exposted and the currents in the intervening channels strengthened when enhanced winter monsoon winds occurred.

It has been globally established that the interglacial bank-derived aragonite Sr-rich export during the mid Brunhes was not fully preserved on slopes and basins adjacent to carbonate banks in intermediate water depths such as in the Maldives Inner Sea at ODP Site 716 and in the Bahamas ODP Site 633 (Droxler et al., 1990). Mid Brunhes low preservation of aragonite was also observed at ODP Site 716 in the Inner Sea based upon the preservation of pteropod tests (Cullen and Droxler, 1990). Moreover, Mid Brunhes planktic calcite accumulation also displays preferential dissolution at intermediate and abyssal depths (Barker et al., 2006; Bassinot et al., 1995). Atoll-derived Sr-rich aragonite interglacial highstand maximum export was obviously not always recorded because dissolution inhibited its accumulation.

The percent of whole pteropods is used as a carbonate dissolution index (Haddad and Droxler, 1996). Decreasing values of the pteropods ratio (whole pteropods / whole pteropods + fragments), therefore, correspond to decreasing preservation or dissolution. Results from piston core 1120 indicated that a major aragonite dissolution interval occurs approximately between 350 and 600 ka, with dissolution maxima occurring at the end of MIS 15, middle of MIS 13 and at the peak of MIS 11 (Fig. 14F). The poorest aragonite preservation, observed in core 1120 between 0.3 and 0.6 Ma, often referred as the mid-Brunhes dissolution interval, is part of a longer 500 ky carbonate dissolution supercycle

(Barker et al., 2006; Bassinot et al., 1995; Droxler et al., 1990; Peterson and Prell, 1985).The mid Brunhes dissolution interval apparently could also explain the decrease of the sediment coarse fraction cycle amplitude during that particular time (Fig. 14B) and to have indirectly influenced the seismic response of this particular part of the sediment column (see below Unit II in Figures 19 and 20).

6.2 **Seismic Analyses and Interpretation**

Multi-channel GI seismic lines and sub-bottom Parasound profiles were acquired during the 2007 NEOMA cruise in the area of the drifts (Fig. 5). Data processing and visualization were carried out by means of Seismic Unix and Petrel (Schlumberger) (Furstenau et al., 2009; Betzler et al., 2009 and 2012). Seismic interpretation was based on available line corresponding to the study area, following the basic concepts of seismic stratigraphy, such as reflectors termination patterns and sequence geometry and organization.

A first seismic analysis of the available Parasound profile P4, a dip line crossing the drifts on top of which cores 1144, 1120 and 1121 are located, illustrates the overall contrasting lithologies between the muddy and sandy drifts (Fig. 17). Because the 4 kHz signal, generated by the energy source of the Parasound sub-bottom profiler, could not penetrate the sandy drift, it is assumed that the coarse sand deposits, encountered in box core 1121 (Fig. 7), most likely represent the main lithology of the 200 m-thick sandy drift (Fig. 17A). On the muddy drift per se, represented by core 1144 in which the overall coarse sediment proportions are minimum relative to cores 1120 and 1121, the sound penetrated as much as 100 m, whereas the sound penetrated only 50 m at the level of the

muddy drift moat where core 1120 is located, characterized by coarse sediment values intermediate between cores 1144 and 1121 (Fig. 17A). The P4 seismic line shows between both cores 1144 and 1120 a clear sequence of continuous and closely spaced parallel reflectors (Figs. 17 B&C). In general, reflectors vary in intensity and strong reflectors are easily traceable between both cores, identifying different units. The seismic line clearly illustrates how a thick unit well imaged on the muddy drift, where core 1144 is located, thin and pinch out towards the drift moat in which core 1120 is positioned and the sandy drift (Fig. 17).

Figure 18 shows a seismic interpretation of line P4, crossing the carbonate juxtaposed muddy and sandy drifts. Interpreted units were defined following stratigraphic analysis, seismic reflector terminations, and strong amplitud reflectors. The sandy drift is composed of three main units, the oldest identified as unit I (Fig. 19A) . In the carbonate sandy drift, the youngest prograding unit (identified as unit III and collored yellow in Figs. 17, 18, and 19), corresponding to the interval studied in piston cores 1120 and 1144, is illustrated by interval colored yellow (Fig. 18A). Unit III is divided into five prograding sub-units represented by clinoforms that can be extended in a basinward direction, toward the muddy drift (Fig. 18B).

Figure 19 shows an interpreted segment of seismic line P4 in which the three main units (Unit I, II and III, blue, brown, and yellow) are identified in the sandy drift based on strong-amplitude reflectors binding them (Fig. 19 A&B). The identified units can be tied to the litho- and chrono-stratigraphies developed in piston cores 1120, 1144, and ODP Site 716, based upon which their ages can be estimated. The upper 14.8 and

12.7 m of the sedimentary column in Unit III at the location of cores 1120 and 1144 represent about 750 ky of the sediment accumulated in the muddy drift moat and about 390 ky on the muddy drift itself, respectively (figs. 10 & 15). The above-mentioned five sub-units (Unit III) can be

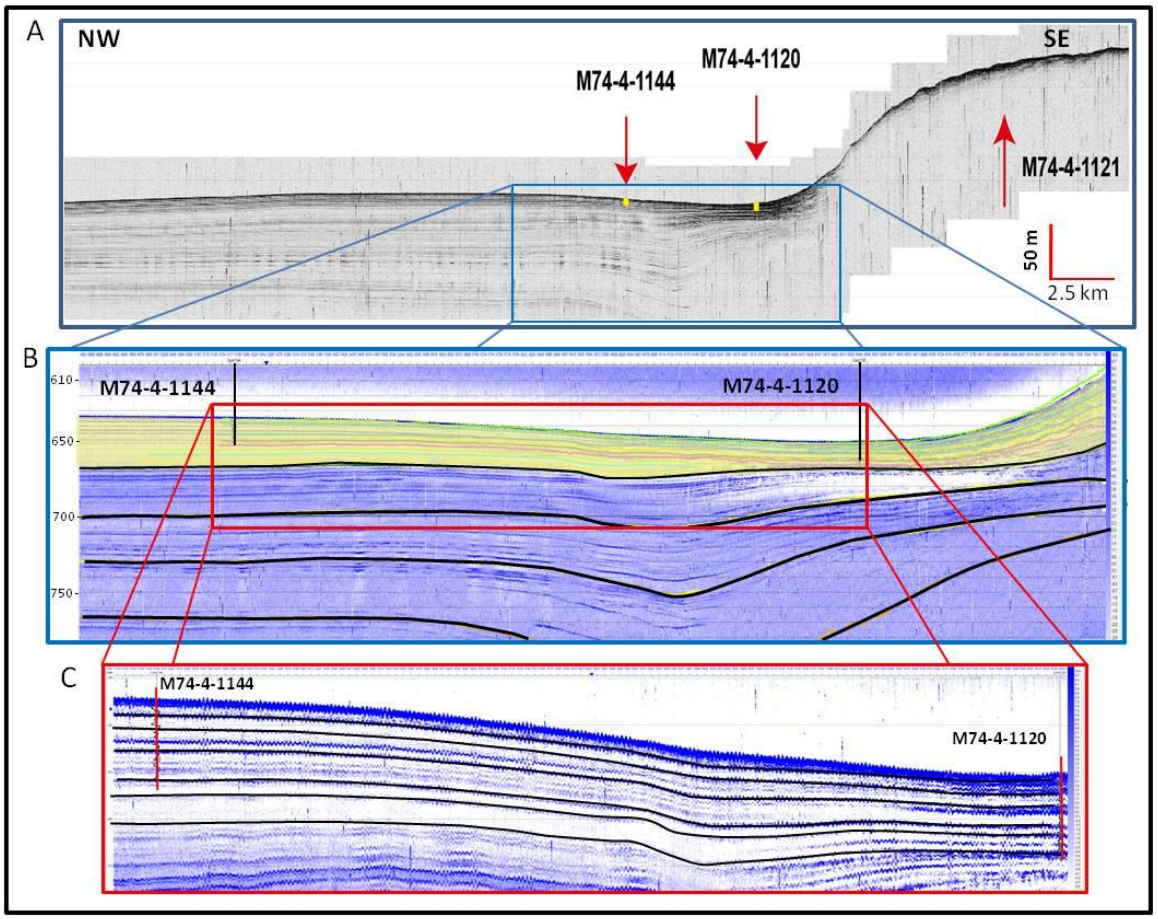

Figure 17. **A.** Uninterpreted parasound sub-bottom profile, segment of line P4, across the carbonate muddy drift and sand drifts (see figure 5 for line location). Note the limited sound penetration on the sandy drift where the M74-4-1121 box core is located. On the muddy drift, the sound penetration is as deep as 100 m, whereas the sound penetrated only 50 m at the level of the drift moat where core M74-4-1120 is located. **B.** Overall interpretation of the muddy drift, yellow shaded unit corresponds to the study interval. **C.** Close view between the two piston cores correlation, seismic profile on the muddy drift shows the continuous, closely spaced, parallel reflectors. Note: see larger version of figure 17 in Appendix I and IB & C.

identified by the ultra-high resolution seismic data processing method developed by Lumina, Geophysical, LLC based upon spectral inversion (Puryear and Castagna, 2008), enhancing the hidden high frequencies (300 and 500 kHz) in the data set.

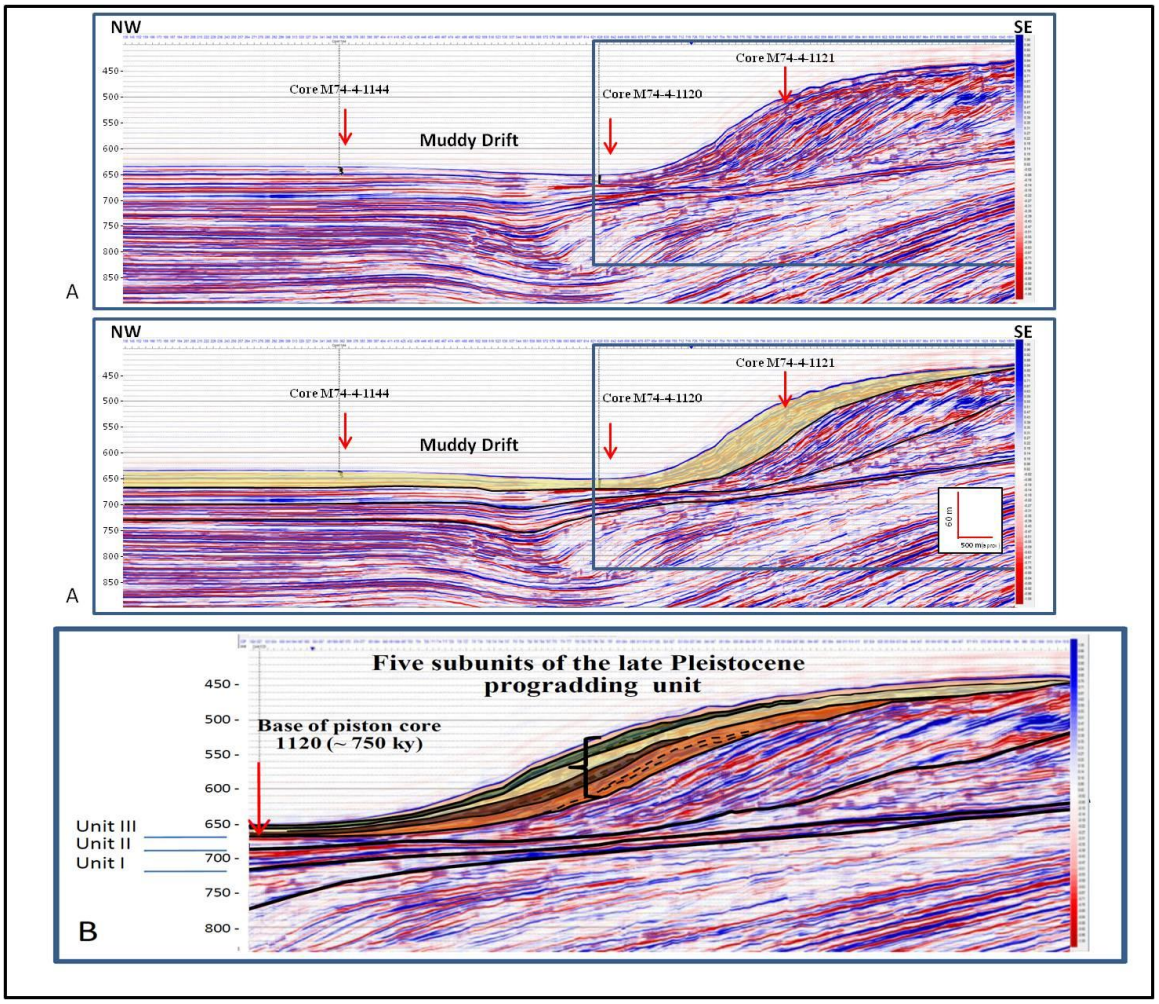

Figure 18 . Ultra spectral inversion high resolution seismic at 300 Hz re-procesed by Lumina, Geophysical (Puryear and Castagna, 2008). **A.** Uninterpreted and interpreted segment of line P4, crossing the carbonate muddy and sandy drifts, yellow shaded Unit III corresponds to the interval incuding the results for the core analyses. **B.** Close view of the main progradding units in the carbonate sandy drift. Five distintic progradding sub-units in the late Pleistocene Unit III are identified by different shades colors. Note: see larger version of figure 18 in Appendix II.

The strongest reflectors (red negative polarity) identified in Unit III on the seismic line reprocessed at 500 Hz, delineated five sub-units and were linked to core 1120 lithologic variations, more precisely to the available coarse fraction downcore cyclic variations. The core lithology was tied to the seismic image using a constant velocity of 1600 m/s (Fig. 20).

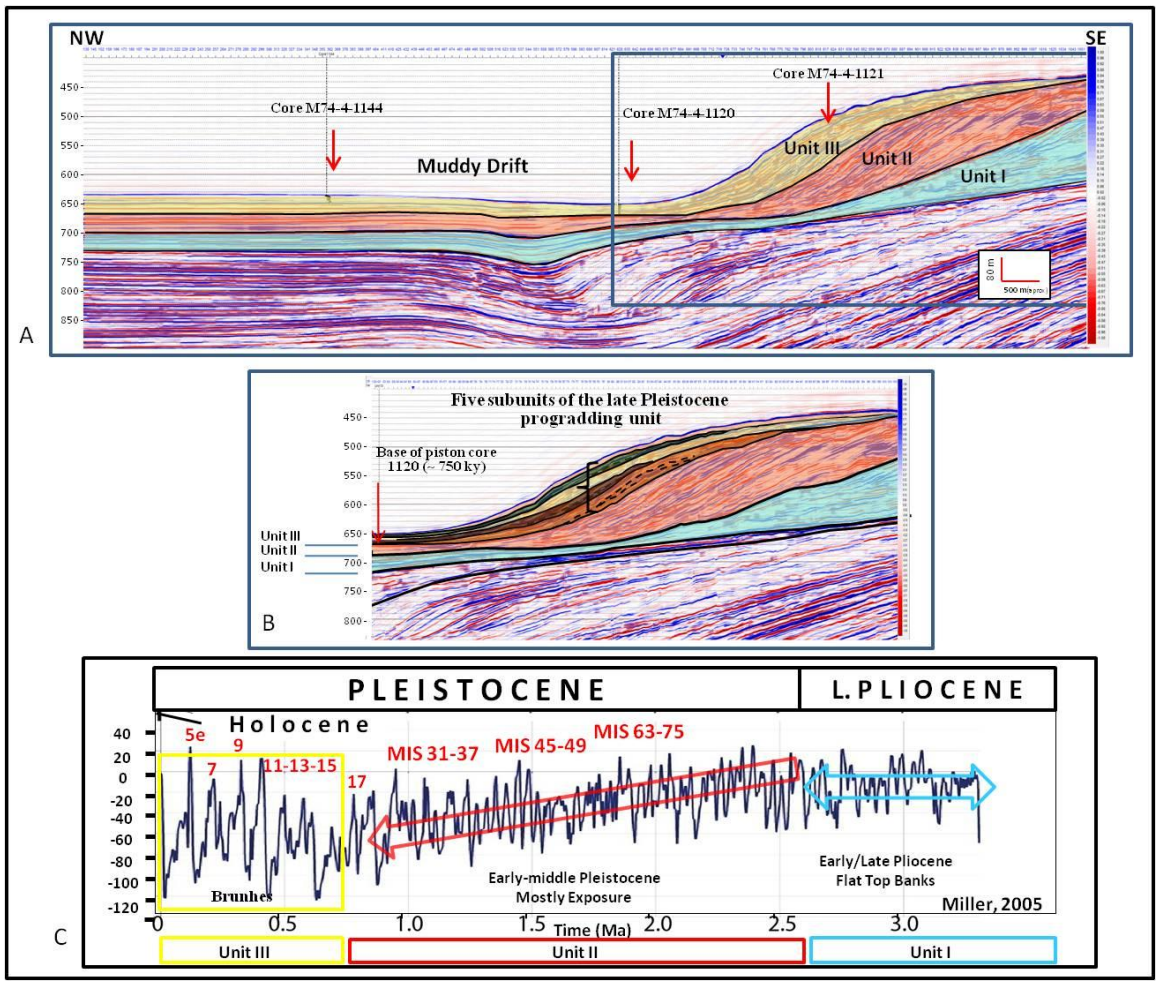

Figure 19. Model for the sandy drift evolution. A and B. Ultra spectral inversion high resolution seismics at 300 Hz re-procesed by Lumina, Geophysical (Puryear and Castagna, 2008). **A.** Interpreted segment of seismic line P4 in which three units (I, II, and III) can be identified in the sandy drift. Their ages were estimated by the chronology in piston core 1120 and ODP Site 716. The age of the lower unit (Unit I) is estimated to be

late Pliocene, and the age of the upper two units (Unit II and III) to be Pleistocene. **B.** The youngest progradding main unit III , made of five subunits, corresponds to the last 740 ky, based on the correlation with the base of piston core 1120. These subunits would then correspond to the five main interglacial highstand intervals (MIS 17, MIS-15 to 11, MIS-9, MIS 7 and MIS-5, as shown in **C**). The underlying Pleistocene unit (Unit II) (shown in A and B) are interpreted to represent unusually strong interglacial highstand intervals (i.e. MIS-31-37and MIS-45-49) as shown in **C**.

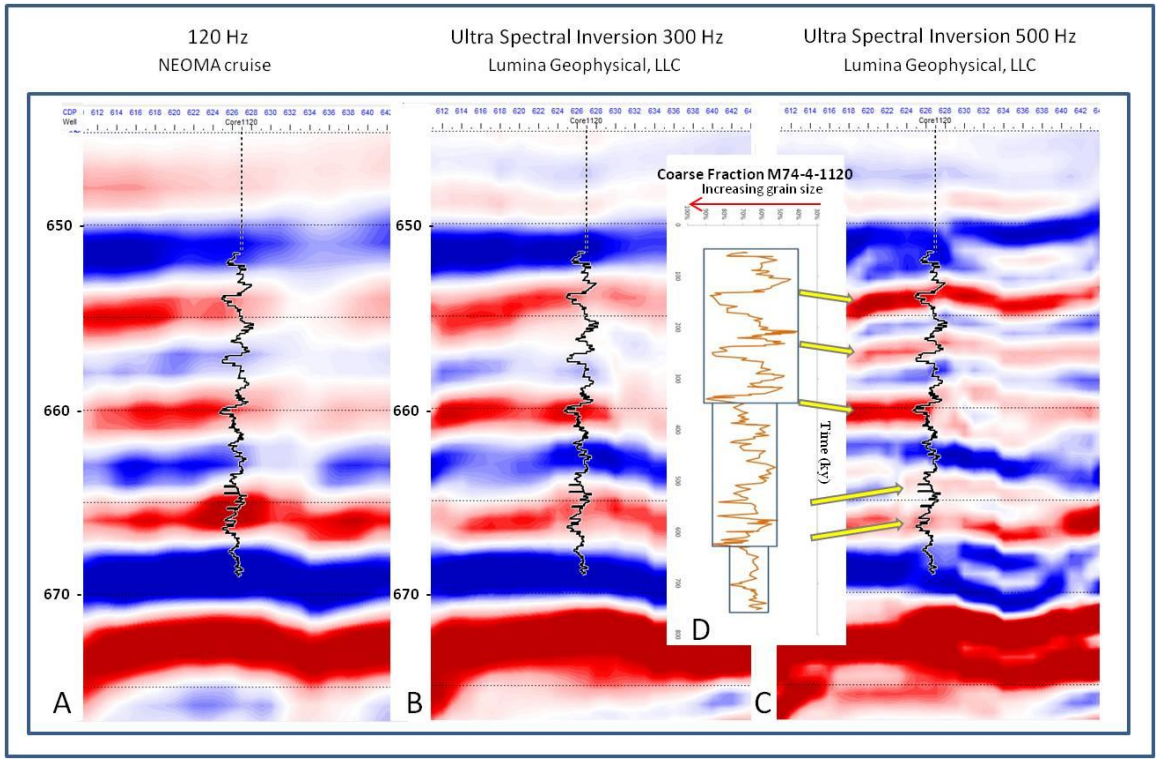

Figure 20. P-4 line segment crossing piston core 1120 processed at three different resolution is used to link the piston core analysis (coarse fraction) with the seismic. Core 1120 litho and chrono-stratigraphies can be linked to the identified five late Pleistocene sub-units in Unit III. **A.** Original data from the NEOMA cruise, frecuency seismic data at 120 Hz. **B - C**. Ultra spectral inversion high resolution seismics at 300 and 500 Hz re-procesed by Lumina, Geophysical (Puryear and Castagna, 2008).

The five main seismic reflectors (red negative polarity) on the seismic line reprocessed at 500 Hz appear to correspond to levels in core 1120 where the strongest

contrast exists between units with low and high coarse fraction (high and low Sr, respectively) mostly at terminations MIS 6/5, 8/7, 10/9, middle 13, and 16/15 (Figs. 20C & 21). Intervals with high coarse fraction content and low Sr atoll-derived fine aragonite, would easily be partially cemented (Fig. 21) and, therefore, yield high seismic velocity as in the periplatform ooze of Northwest Providence Channel (Bahamas) (Fig. 22; (Slowey et al., 1989).

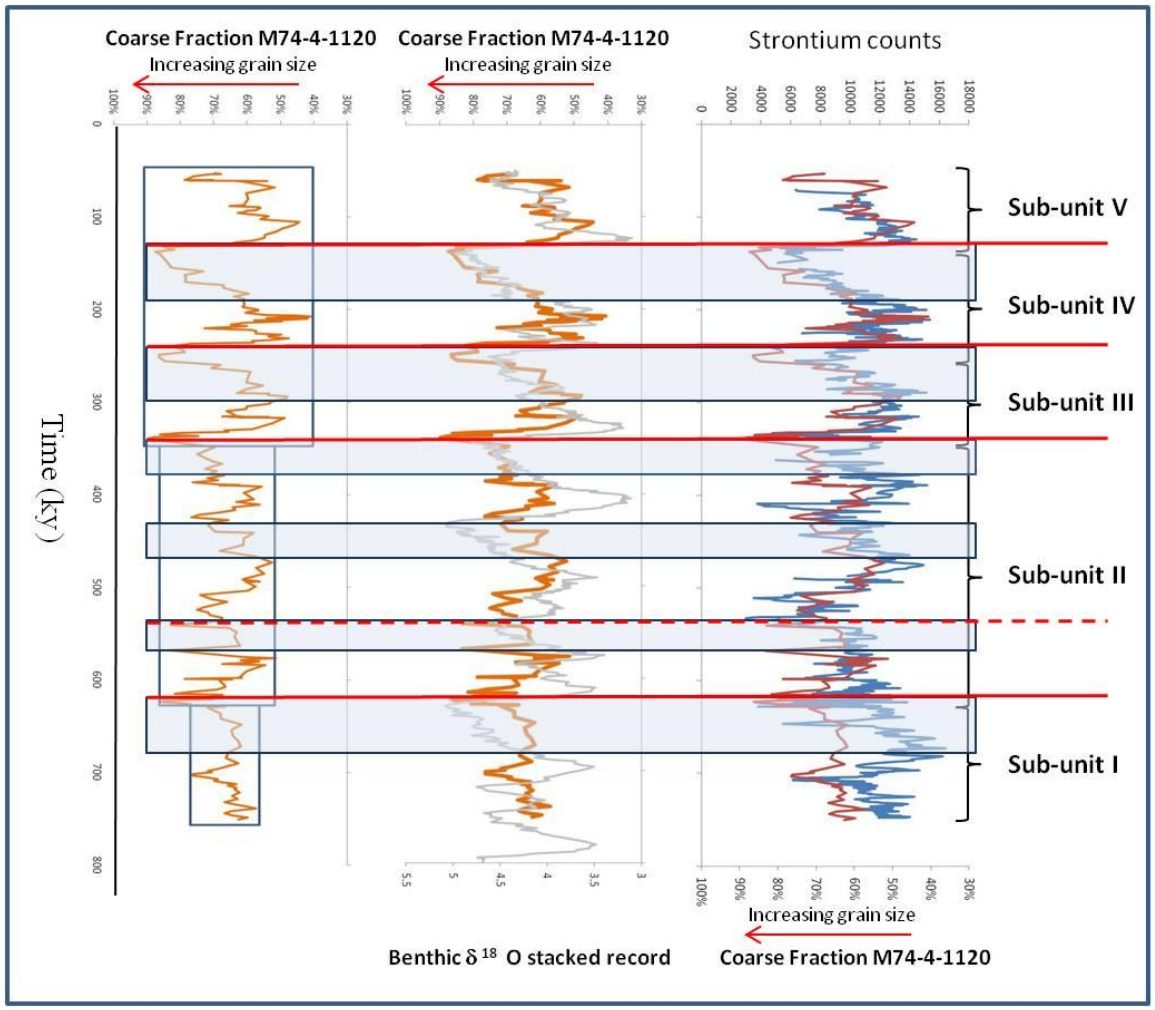

Figure 21. Chronostratigraphy identification of five sub-units based on the coarse fraction and strontium counts from piston core 1120.

The older part of the muddy drift can be correlated with stratigraphies established at ODP Site 716, located 15 km to the northwest (Betzler, et al., 2012, Fig. 5). The two lower drift units (Unit I light blue and II brown in Figs. 19A&B) were identified based on the strong-amplitude reflector and dated by correlation to ODP Site 716, as late Pliocene (Unit I) and early-middle Pleistocene (Unit II) (Fig. 19 A&B).

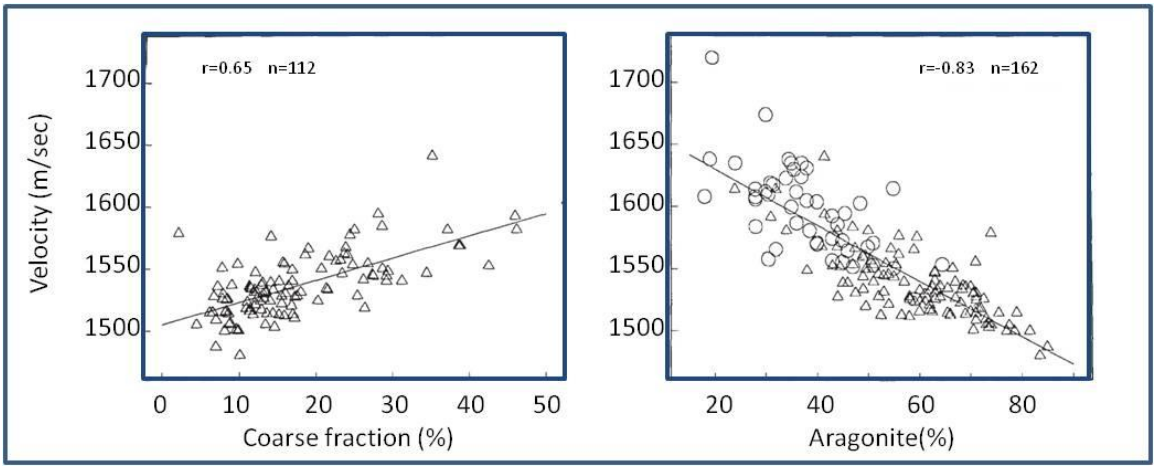

Figure 22. Plots of coarse fraction and aragonite content (%) versus *in situ* compresional velocity (m/sec). Higher velocities correspond to high coarse size fraction and low fine aragonite content. (Modified from Slowey, et al., 1989)

Model for the sandy drift evolution was developed based on the interpretation of the available multi-channel seismic linked to the lithology variations and stratigraphy developed in the available piston cores. Observations of NEOMA high resolution MCS dip and strike lines (Fig. 5A) show that the upper third of the sandy drift (Unit III), composed of five distinct wedge-like main sub-units downlapping on a series of unconformities, thins on the toe of the muddy drift front into a very recent sequence not much thicker than 15-20 m (Fig. 18). This thin unit represents the upper part of a low

relief muddy drift that contemporaneously accumulated adjacent to the sandy drift. The lower two third of the sandy drift (Units II and I) thins into an underlying unit not thicker than tens of meters (Fig. 19).

The age of the lower unit I of the sandy drift is estimated to be late Pliocene, and the age of the upper two units II and III to be early-middle and late Pleistocene, respectively (Fig. 19C). The youngest prograding unit III, made of five sub-units, corresponds to the last 750 ky (almost the full Bruhnes), based on the correlation with the base of core 1120. These subunits could then correspond to the five main interglacial highstand intervals (MIS 17, MIS 1513-11, MIS 9, MIS 7, and MIS 5, as shown in Figure 19C). Based upon these observations, the accumulation of the large and thick deep carbonate drift northwest of Gaafaru Falhu atoll was most likely initiated during the late Pliocene (Fig. 19C).

6.3 **Sandy Drift Evolution and Timing**

Interpretation of the P4 seismic line shows that the upper third of the sandy drift, interval related to the studied section penetrated by piston cores 1120 and 1144, is composed of five distinct wedge-like main subunits downlapping on a series of unconformities into the muddy drift. Based on planktic foraminiferal oxygen isotope analysis and the correlation with the benthic foraminifer oxygen isotope stacked LR04 curve (Lisiecki and Raymo, 2005), the base of these subunits corresponds to the last 750 ky, These subunits correspond to the carbonate sediments that accumulated during several strong interglacial highstand intervals MIS 17, 15/13/11, 9, 7 and 5. (Fig. 19). Exporting of these fine sediments would then be related to the flooding events of exposed

atoll top during intervals of rising sea-level and highstand (Figs. 20&21). The periodicity of these sea-levels fluctuations is closely to the 100.000 years climate cycle, in particular during the middle and late Brunhes. It is assumed that the thin units separating these highstand intervals correspond to minimum sediment accumulation, even non deposition, or even partial erosion that would have occurred during periods of lowstand, when a drop in sea-level turned off the export of carbonate fine sediment and stronger channel currents were initiated by enhanced winter monsoonal winds during glacial intervals (Zhisheng et al., 2011). In order to understand better the deep sandy drift evolution in this particular location of the Maldives Inner Sea, deeper cores will be essential to fully develop a comprehensive interpretation of the evolution of the drift during the late Pliocene and Quaternary.

7. Conclusions

- Based upon the interpretation of a new multi beam and high resolution multi channel seismic data sets, two piston cores and one box core collected in my study area during the 2007 NEOMA expedition on the R/V *Meteor*, the overall Plio-Quaternary evolution of a juxtaposed set of sandy and muddy deep water carbonate drift is better understood.
- 18 MIS $\delta^{18}O$ events, defined and tied to a specific age on the LR 04 stacked curve, are identified in two high resolution oxygen isotope records [*G. ruber* (white)], produced in both piston cores 1120 and 1144 from the muddy carbonate drift. Core 1120 is interpreted to represent the initiation of glacial MIS 18, and,

therefore, the core has recovered a sediment interval representing about the last 750 ky or almost the entire Brunhes period. The bottom of core 1144 is interpreted to occur at the beginning of the second part of MIS 11, representing event MIS 11.24 or 391 ky. Because lengths of both cores 1120 and 1144 (14.73 and 12.86 m, respectively) are about the same, the sedimentation rates are twice higher on the center of the muddy drift (core 1144) than on the muddy drift moat (core 1120). Bottom currents, assumed to be maximum within the drift moat, would winnow fine sediment and explain the reason why the sediment coarse fraction is systematically higher in core 1120 from the drift moat than in core 1144 from the center of the muddy drift.

- High resolution downcore variations of Sr counts versus time, an excellent proxy for the input of fine bank-derived aragonite produced from the adjacent atoll neritic environments, display, in both cores 1120 and 1144, a cyclic glacial-interglacial pattern generally in phase with the planktic foraminifer oxygen isotope records. This relationship, is especially clear during the late Brunhes (the last three glacial cycles) during which the highstand shedding concept is well-developed in both cores. However, this relationship becomes tenuous in the early and middle Brunhes during which minima of bank-derived Sr-rich aragonite accumulation occurred during interglacials/highstands (MIS 11 and 13) and maxima during glacial/lowstands (MIS 14 and 16). These observations are not unexpected, because similar out of phase relationship has been globally observed on slopes and basins adjacent to carbonate banks at intermediate water depths during the mid Brunhes. It can be concluded that interglacial bank-derived

aragonite Sr-rich export during the mid Brunhes was not fully preserved on the muddy carbonate drift. These out of phase relationship is strengthened by the downcore variations of percent of whole pteropods used as a carbonate dissolution index. Maximum pteropods fragmentation or poorest aragonite preservation, observed in core 1120 between 0.3 and 0.6 Ma, often referred as the mid-Brunhes dissolution interval, is part of a Quaternary 500 ky-long carbonate dissolution supercycle.

- When compared with the sea-level curve of Miller, et al. (2011), maximum Sr-rich fine sediment accumulation on the Inner Sea drifts occurred when atoll tops were flooded during the late Brunhes interglacial sea-level highstands and export of fine bank-derived Sr-rich neritic aragonite sediments was maximum. This export became minimum during glacial sea-level lowstands when the atoll lagoons were exposed. The highstand shedding of fine bank-derived Sr-rich aragonite towards the muddy drift dilute the coarse sediment fraction, consists mostly of planktic foraminifer and pteropods tests, enhancing alternating interglacial thick intervals characterized by low coarse sediment fraction values with glacial thin intervals characterized by high coarse sediment fraction. This lithologic contrast, most likely also amplified by preferential fine sediment winnowing by strengthened glacial bottom currents, generate impedance contrast sufficient to generated seismic reflectors in the high resolution multi-channel seismic lines imaging the muddy carbonate drift. Once the core lithologies were tied to the seismic data sets, information gathered in cores 1120 and 1144 were

used to develop our understanding of the nature and evolution of the juxtaposed muddy and sandy carbonate drifts.

- Three main seismic units (Unit I, II and III) were identified in the sandy drift based on conspicuous strong-amplitude reflectors bounding these units. The identified units were tied to the litho- and chrono-stratigraphies developed in piston cores 1120, 1144, and ODP Site 716. Five sub-units were identified in the late Pleistocene Unit III on the ultra-high resolution seismic data, when processed through a spectral inversion method by Lumina, Geophysical, LLC. The five main seismic reflectors (red negative polarity) on the seismic line reprocessed at 500 Hz were linked to core 1120 coarse fraction downcore cyclic variations. This interval appear to correspond to levels in core 1120 where the strongest contrast exist between units with low and high coarse fraction mostly at Terminations MIS 6/5, 8/7, 10/9, middle 13, and 16/15. The two lower units (Unit I and II) were identified based on the strong-amplitude reflector and dated by correlation to ODP Site 716, as late Pliocene (Unit I) and early-middle Pleistocene (Unit II).
- Model for the sandy drift evolution was developed based on the interpretation of the available multi-channel seismic linked to the stratigraphy. The age of the lower unit I of the sandy drift is estimated to be late Pliocene. This youngest prograding unit III, corresponds to the last 750 ky (Bruhnes Period), based on the correlation with the base of core 1120. The five distinct wedge-like main subunits identified in Unit III are downlapping on a series of unconformities into the muddy drift; these subunits correspond to distinct carbonate accumulation packages that occurred during strong interglacial highstand intervals, MIS 17, 15-

13-11, MIS 9, MIS 7, and MIS 5. The age of the upper two units II and III are estimated to be early-middle and late Pleistocene, respectively. Based on my study, the evolution of the deep carbonate drift at Gaafaru Falhu atoll was most likely initiated during the late Pliocene.

- Overall, late Plio-Quaternary sea level fluctuations during the last 3.0 My influenced the evolution of the sandy and muddy drifts northwest of Gaafaru Falhu Atoll at different time scales. Based upon the results of my research, it is difficult to assess the effect of variable monsoonal deep water currents on the evolution of the deep carbonate drifts at glacial and interglacial time scale or through the last 3.0 My. Stronger channel currents initiated by enhanced glacial winter monsoonal winds could explain contemporaneous large coarse sediment fraction concentration and some of the observed sediment erosions on the prograding sub-units of late Pleistocene Unit III.
- My research results clearly show that linking lithological variations in two piston cores, though only limited in lengths to 12-14 m, to the high and ultra high-resolution seismic images of the muddy drift is indispensable to directly understand the late Pleistocene development of the muddy drift and indirectly to establish the late Pleistocene evolution of the adjacent sandy drift. Obviously, recovering through drilling late Pliocene/Quaternary sedimentary sequences would greatly improve our understanding of the muddy and sandy drift full evolution. Moreover this model should not only be limited to the interpretation of a 2D cross section, but rather be developed in 3D seismic images to fully comprehend the complex sedimentary processes linked to the drift edification in

the context of sea level fluctuations and climatic monsoonal bottom current variations in the context of the initiation and strengthening of the Northern Hemisphere Plio-Quaternary glaciations.

References

Aubert, O., and A. Droxler, 1996, Seismic stratigraphy and depositional signatures of the Maldive carbonate system (Indian Ocean): Marine and Petroleum Geology, v. 13, p. 503-536.

Aubert, O., and A. W. Droxler, 1992, General Cenozoic Evolution of the Maldives Carbonate System (Indian Ocean): Centres de Recherches Exploration-Production Elf-Aquitaine, v. 16, p. 113-136.

Backman, J., R. A. Duncan, and et al., 1988, Proc. ODP. Init. Repts, College Station, TX (Ocean Drilling Program).

Barker, S., D. Archer, L. Booth, H. Elderfield, J. Henderiks, and R. E. M. Rickaby, 2006, Globally increased pelagic carbonate production during the Mid-Brunhes dissolution interval and the CO2 paradox of MIS 11: Quaternary Science Reviews, v. 25, p. 3278-3293.

Bassinot, F. C., L. Beaufort, E. Vincent, L. D. Labeyrie, F. Rostek, P. J. Muller, X. Quidelleeur, and Y. Lancelot, 1995, Coarse fraction fluctuations in pelagic carbonate sediments from the tropical Indian Ocean: A 1500-kyr record of carbonate dissolution: Paleoceanography, v. 9, p. 579-600.

Belopolsky, A., and A. W. Droxler, 2003, Imaging Tertiary carbonate system-the Maldives, Indian Ocean: Insights into carbonate sequence interpretation: The Leading Edge, v. 22.

Belopolsky, A., and A. W. Droxler, 2004b, Seismic Expressions of Prograding Carbonate Bank Margins: Middle Miocene Progradation in the Maldives, Indian Ocean. : American Association of Petroleum Geologists v. 81.

Betzler, C., J. Furstenau, T. Ludmann, C. Hubscher, S. Lindhorst, A. Paul, J. J. G. Reijmer, and A. W. Droxler, 2012, Sea-level and ocean-current control on carbonate-platform growth, Maldives, Indian Ocean: Basin Research, v. 24, p. 1-25.

Betzler, C., C. Hubscher, S. Lindhorst, J. J. G. Reijmer, M. Romer, A. W. Droxler, J. Furstenau, and T. Ludmann, 2009, Monsoon-induced partial carbonate platform drowning (Maldives, Indian Ocean): Geology, v. 37, p. 867-870.

Boardman, M. R., A. C. Neumann, P. A. Baker, L. A. Dulin, R. J. Kenter, G. E. Hunter, and K. B. Kiefer, 1986, Banktop responses to Quaternary fluctuations in sea level recorded in periplatform sediments: Geology, v. 14, p. 28.

Cullen, J. L., and A. W. Droxler, 1990, Late Quaternary variations in planktonic foraminifer faunas and pteropod preservation in the Equatorial Indian Ocean. , *in* B. J. Duncan RA, Peterson, LC., et al., , ed., Proceding of the Ocean Drilling Program, Scientific Results: College Station, p. 579-588.

DeMets, C., R. G. Gordon, and J.-Y. Royer, 2005, Motion between the Indian, Capricorn and Somalian plates since 20 Ma: implications for the timing and magnitude of distributed lithospheric deformation in the equatorial Indian ocean: Geophysical Journal International, v. 161, p. 445-468.

Droxler, A. W., G. A. Haddad, D. A. Mucciarone, and J. L. Cullen, 1990, Pliocene-Pleistocene aragonitic cyclic variations in Ocean Drilling Program holes 714 A and 716B (The Maldives) compared to hole 633 A (Bahamas): Records of climatic-induced CaCO3 preservation at intermediate water depths:, Procedings of the Ocean Drilling Program, Scientific Results: Ocean Drilling Program, Texas A&M University, College Station, Texas.

Droxler, A. W., W. Schlager, and C. C. Whallon, 1983, Quaternary aragonite cycles and oxygen-isotope record in Bahamian carbonate ooze. : Geological Society of America Bulletin, v. 11, p. 235-239.

Dunbar, G. B., and G. R. Dickens, 2003, Late Quaternary schedding of shallow-marine carbonate along a tropical mixed siliciclastic-carbonate shelf: Great Barrier Reef, Australia: Sedimentology, v. 50, p. 1061-1077.

Duncan, R. A., and R. B. Hargraves, 1990, $^{40}Ar/^{39}Ar$ Geochronology of Basement Rocks From the Mascarene Plateau, The Chagos Bank, and The Maldives Ridge: Proceedings of the Ocean Drilling Program, Scientific Results, v. 115.

Furstenau, J., S. Lindhorst, C. Betzler, and C. Hubscher, 2009, Submerged reef terraces of the Maldives (Indian Ocean): Geo-Marine, v. 30.

Gischler, E., J. H. Hudson, and A. Pisera, 2008, Late Quaternary reef growth and sea level in the Maldives (Indian Ocean): Marine Geology, v. 250, p. 104-113.

Gordon, R. G., C. DeMets, and J.-Y. Royer, 1998, Evidence for long-term diffuse deformation of the lithosphere of the equatorial Indian Ocean: Nature, v. 395, p. 370-374.

Haddad, G. A., and A. W. Droxler, 1996, Metastable CaCO3 dissolution at intermediate water depths of the Caribbean and western North Atlantic: Implications for intermediate water circulation during the past 200,000 years: Paleoceanography, v. 11, p. 701-716.

Kendall, C. G. S. C., and W. Schlager, 1981, Carbonates and relative changes in sea level: Marine Geology, v. 44, p. 181-212.

Malone, M. J., P. A. Baker, S. J. Burns, and P. K. Swart, 1990, Geochemistry of periplatform carbonate sediments, Leg 115, Site 716 (Maldives Archipelago, Indian Ocean): Proceedings of the Ocean Drilling Program, Scientific Results: Ocean Drilling Program, College Station, Texas, Texas A&M University, p. 647-659.

Miller, K. G., G. S. Mountain, J. D. Wright, and J. V. Browning, 2011, A 180-million-year record of sea level and ice volume variations from continental margin and deep-sea isotopic records: Oceanography, v. 24, p. 40-53.

Naseer, A., and B. G. Hatcher, 2004, Inventory of the Maldives? coral reefs using morphometrics generated from Landsat ETM+ imagery: Coral Reefs, v. 23, p. 161-168.

Nicora, A., and I. P. Silva, 1990, Paleogene shallow-water lager foraminifera from holes 714 A and 715A, Leg 115, Indian Ocean, in R. A. Duncan, J. Backman, L.C. Peterson, et al., , *in* T. A. M. University, ed., Proceedings of the Ocean Drilling Program, Scientific Results:Ocean Drilling Program, College Station, Texas, 115, p. 381-393.

Peterson, L. C., and W. L. Prell, 1985, Carbonate dissolution in Recent sediments of the eastern equatorial Indian Ocean: Preservation and carbonate loss above the Iysocline: Marine Geology, v. 64, p. 259-290.

Purdy, E., 1974a, Karst-Determined Facies Patterns in British Honduras: Holocene Carbonate Sedimentation Model: American Association of Petroleum Geologists, v. 58.

Purdy, E. G., and G. T. Bertram, 1993, Carbonate concepts from the Maldives, Indian Ocean. , AAPG Studies in Geology, Tulsa, Oklahoma, p. 56.

Puryear, C., I, and J. P. Castagna, 2008, Layer-thickness determination and stratigraphic interpretation using spectral inversion: Theory and application: Geophysics, v. 73, p. 37-48.

Reymer, J. J. G., Wolfgang Schlager, and A. W. Droxler, 1988, Site 632 Pliocene-Pleistocene Sedimentation Cycles in a Bahamian Basin. In Austin, J. A., Schlager, W., et al., Proc. ODP, Sci. Results, College Station, TX, p. 213-220.

Sarkar, S., and A. K. Gupta, 2009, Deep-sea paleoceanography of the Maldives Islands (ODP Hole 716A), equatorial Indian Ocean during MIS 12-6: Journal of Bioscience, v. 34.

Schlager, W., 2005, Carbonate sedimentology and sequence stratigraphy: Soc. Sedim. Geol., Concepts Sedimentol. Paleontol, v. 8, p. 200.

Schlager, W., J. J. G. Reijmer, and A. W. Droxler, 1994, . Highstand Shedding of carbonate platform: Sedimentary Research, v. 64, p. 270-281.

Slowey, N. C., A. C. Neumann, and K. C. Baldwin, 1989, Seismic expression of Quaternary climatic cycles in the peri-platform carbonate ooze of the northern Bahamas: Geological Society of America Bulletin, v. 101, p. 1563-1573.

Thompson, P. R., A. W. H. Be, J.-C. Duplessy, and N. J. Shackleton, 1979, Disappearance of pink-pigmented Globigerinoides ruber at 120,000 yr BP in the Indian and Pacific Oceans: Nature, v. 280, p. 554-558.

Tomczak, M., and J. S. Godfrey, 2003, Regional oceanography: An introduction, Delhi, Daya, 390 p.

Woodroffe, C. D., 2005, Late Quaternary sea-level highstands in the central and eastern Indian Ocean: A review: Global and Planetary Change, v. 49, p. 121-138.

Woodroffe, C. D., 2008, Reef-island topography and the vulnerability of atolls to sea-level rise: Global and Planetary Change, v. 62, p. 77-96.

Zheng, F., Q. Li, B. Li, M. Chen, X. Tu, J. Tian, and Z. Jian, 2005, A millennial scale planktonic foraminifer record of the mid-Pleistocene climate transition from the northern South China Sea: Palaeogeography, Palaeoclimatology, Palaeoecology, v. 223, p. 349-363.

Zhisheng, A., S. C. Clemens, J. Shen, X. Qiang, Z. Jin, Y. Sun, W. L. Prell, J. Luo, S. Wang, H. Xu, Y. Cai, W. Zhou, X. Liu, W. Liu, Z. Shi, L. Yan, X. Xiao, H. Chang, F. Wu, L. Ai, and F. Lu, 2011, Glacial-Interglacial Indian Summer Monsoon Dynamics: Science, v. 333, p. 719-723.